Multi-Stage Modification of the Northern Slave Mantle Lithosphere: Evidence from Zircon- and Diamond-Bearing Eclogite Xenoliths Entrained in Jericho Kimberlite, Canada

LARRY M. HEAMAN[1]*, ROBERT A. CREASER[1], HARRISON O. COOKENBOO[2] AND TOM CHACKO[1]

[1]DEPARTMENT OF EARTH AND ATMOSPHERIC SCIENCES, UNIVERSITY OF ALBERTA, EDMONTON, ALTA., CANADA T6G 2E3

[2]WATTS, GIFFIS, AND McQUAT, 620–475 HOWE STREET, VANCOUVER, B.C., CANADA V6C 4B3

The Jericho kimberlites are part of a small Jurassic kimberlite cluster in the northern Slave craton, Canada. A variety of dating techniques were applied to constrain the nature and age of two Jericho kimberlites, JD-1 (170·2 ± 4·3 Ma Rb–Sr phlogopite megacrysts, 172·8 ± 0·7 Ma U–Pb eclogite rutile, 178 ± 5 Ma U–Pb eclogite zircon lower intercept) and JD-3 (173 ± 2 Ma Rb–Sr phlogopite megacryst; 176·6 ± 3·2 Ma U–Pb perovskite), and all yielded identical results within analytical uncertainty. As there is no discernible difference in the radiometric ages obtained for these two pipes, the composite Rb–Sr phlogopite megacryst date of 173·1 ± 1·3 Ma is interpreted as the best estimate for the emplacement age of both Jericho pipes. The initial Sr isotope composition of 0·7053 ± 0·0003 derived from phlogopite megacrysts overlaps the range (0·7043–0·7084) previously reported for Jericho whole-rocks. These strontium isotope data, combined with the radiogenic initial $^{206}Pb/^{204}Pb$ ratio of 18·99 ± 0·33 obtained in this study, indicate that the Jericho kimberlites are isotopically similar to Group 1 kimberlites as defined in southern Africa. The Jericho kimberlites are an important new source of mantle xenoliths that hold clues to the nature of the Slave craton subcontinental mantle. A high proportion (30%) of the Jericho mantle xenolith population consists of various eclogite types including a small number (2–3%) of apatite-, diamond-, kyanite- and zircon-bearing eclogites. The most striking aspect of the Jericho zircon-bearing eclogite xenoliths is their peculiar geochemistry. Reconstructed whole-rock compositions indicate that they were derived from protoliths with high FeO, Al_2O_3 and Na_2O contents, reflected in the high-FeO (22·6–27·5 wt %) nature of garnet and the high-Na_2O (8·47–9·44 wt %) and high-Al_2O_3 (13·12–14·33 wt %) character of the clinopyroxene. These eclogite whole-rock compositions are highly enriched in high field strength elements (HFSE) such as Nb (133–1134 ppm), Ta (5–28 ppm), Zr (1779–4934 ppm) and Hf (23–64 ppm). This HFSE enrichment is linked to growth of large (up to 2 mm) zircon and niobian rutile crystals (up to 3 modal %) near the time of eclogite metamorphism. The diamond-bearing eclogites on the other hand are characterized by high-MgO (19·6–21·3 wt %) garnet and ultralow-Na_2O (0·44–1·50 wt %) clinopyroxene. Paleotemperature estimates indicate that both the zircon- and diamond-bearing eclogites have similar equilibration temperatures of 950–1020°C and 990–1030°C, respectively, corresponding to mantle depths of 150–180 km. Integration of petrographic, whole-rock and mineral geochemistry, geochronology and isotope tracer techniques indicates that the Jericho zircon-bearing eclogite xenoliths have had a complex history involving Paleoproterozoic metamorphism, thermal perturbations, and two or more episodes of Precambrian mantle metasomatism. The oldest metasomatic event (Type 1) occurred near the time of Paleoproterozoic metamorphism (~1·8 Ga) and is responsible for the extreme HFSE enrichment and growth of zircon and high-niobian rutile. A second thermal perturbation and concomitant carbonatite metasomatism (Type 2) is responsible for significant

*Corresponding author. larry.heaman@ualberta.ca

apatite growth in some xenoliths and profound light rare earth element enrichment. Type 2 metasomatism occurred in the period 1·0–1·3 Ga and is recorded by relatively consistent whole-rock eclogite model Nd ages and secondary U–Pb zircon upper intercept dates. These eclogite xenoliths were derived from a variety of protoliths, some of which could represent metasomatized pieces of oceanic crust, possibly linked to east-dipping subduction beneath the Slave craton during construction of the 1·88–1·84 Ga Great Bear continental arc. Others, including the diamond-bearing eclogites, could be cumulates from mafic or ultramafic sill complexes that intruded the Slave lithospheric mantle at depths of about 150–180 km.

INTRODUCTION

The subcontinental mantle lithosphere beneath stable Archean cratons can extend to depths of >300 km (e.g. Jordan, 1988). Some of these 'cratonic mantle roots' have had a protracted geological history reaching back to at least Mesoarchean times (∼3·5 Ga) based on model Nd and Os age estimates [for a summary see Pearson (1999)]. Although the subcontinental mantle is relatively inaccessible to direct study, it may have a history closely linked to crustal growth and probably plays an important role in stabilizing continental fragments from processes such as subduction and rifting. The nature and origin of cratonic mantle roots remains largely unknown and can only be accessed remotely through seismic or teleseismic studies and more directly through the study of mantle xenoliths entrained in volcanic rocks.

Mantle xenoliths provide us with some indication of the antiquity and composition of the mantle lithosphere and processes involved in modifying this lithosphere through geological time. However, determining mantle xenolith formation ages and the timing of metamorphic and metasomatic events that have affected such xenoliths has long been a challenge because these xenoliths have resided at great depth where temperatures are high enough (>900°C) that diffusion distances for most elements are on the scale of centimeters to meters over a period of a few million years (Pearson, 1999). For example, many of the minerals that occur in mantle xenoliths and are potentially formed during mantle metasomatism and can be dated radiometrically (such as apatite, phlogopite and rutile) all have relatively low closure temperatures to diffusion of daughter products from radioactive decay. Therefore, only the most robust isotopic systems will preserve any pre-eruption age record.

The dominant mantle xenoliths recovered from kimberlites can be broadly subdivided into peridotitic and eclogitic suites. The proportion of each xenolith suite preserved in any kimberlite is variable but peridotite generally dominates. However, a few kimberlites world-wide are renowned for their unusual abundance of eclogite xenoliths, including Roberts Victor, Bellsbank/Bobbejaan (South Africa), Koidu (Sierra Leone), Orapa (Botswana), and several pipes from Yakutia, Russia (e.g. Mir, Udachnaya and Zagadochnaya). The Jericho JD-1 pipe in northern Canada can be added to this list as a North American example of an eclogite-rich kimberlite.

The Jericho JD-1 kimberlite from the northern Slave craton, Canada, contains abundant (30%) bimineralic eclogite xenoliths (Cookenboo, 1998a, 1998b; Cookenboo et al., 1998a; Kopylova et al., 1999a, 2004). In addition, the Jericho eclogite population includes a small proportion (2–3%) that contains both zircon and rutile and one xenolith in our collection that contains abundant apatite, rutile and zircon. Although zircon-bearing eclogite lenses in collisional orogens (orogenic massifs) are relatively common, where both the timing of protolith formation and high-pressure metamorphism are recorded in the U–Pb zircon systematics (e.g. Peucat et al., 1982; Paquette et al., 1985, 1995; Creaser et al., 1997), zircon-bearing eclogites entrained in kimberlites are extremely rare. To our knowledge there are only two mantle xenoliths from any volcanic rock that are reported to contain both zircon and rutile. One is an eclogite (CCS-41) entrained in the Calcutteroo micaceous kimberlite located 230 km north of Adelaide, Australia (Chen et al., 1994), and the other is from a veined harzburgite (LB-17) from the Labait volcano, Tanzania (Rudnick et al., 1998, 1999). More recently, Schmitz et al. (2003) reported U–Pb and Lu–Hf isotope data for zircon isolated from eclogite xenoliths entrained in the Lace and Lovedale kimberlites, South Africa. It should be noted that kimberlite can contain abundant crustal zircon (e.g. from disaggregated crustal xenoliths) and, occasionally, large (centimeter-size) mantle zircon, so it is important to demonstrate that zircons isolated from eclogite actually formed together with the eclogite paragenesis and are not related to zircon xenocrysts derived from infiltrated kimberlite.

In this study we document the mineral chemistry for the zircon- and diamond-bearing eclogite suites at Jericho and attempt to constrain the nature and timing of Jericho kimberlite magmatism using a variety of techniques; these include Rb–Sr dating of kimberlite and eclogite phlogopite macrocrysts, U–Pb dating of eclogite rutile/garnet and kimberlite matrix perovskite. In addition, we attempt to ascertain the nature of the eclogite protoliths and unravel the pre-entrainment metamorphic and metasomatic history of these xenoliths by investigating the Sm–Nd mineral–whole-rock system, U–Pb zircon growth history and the Pb isotope composition of eclogitic apatite.
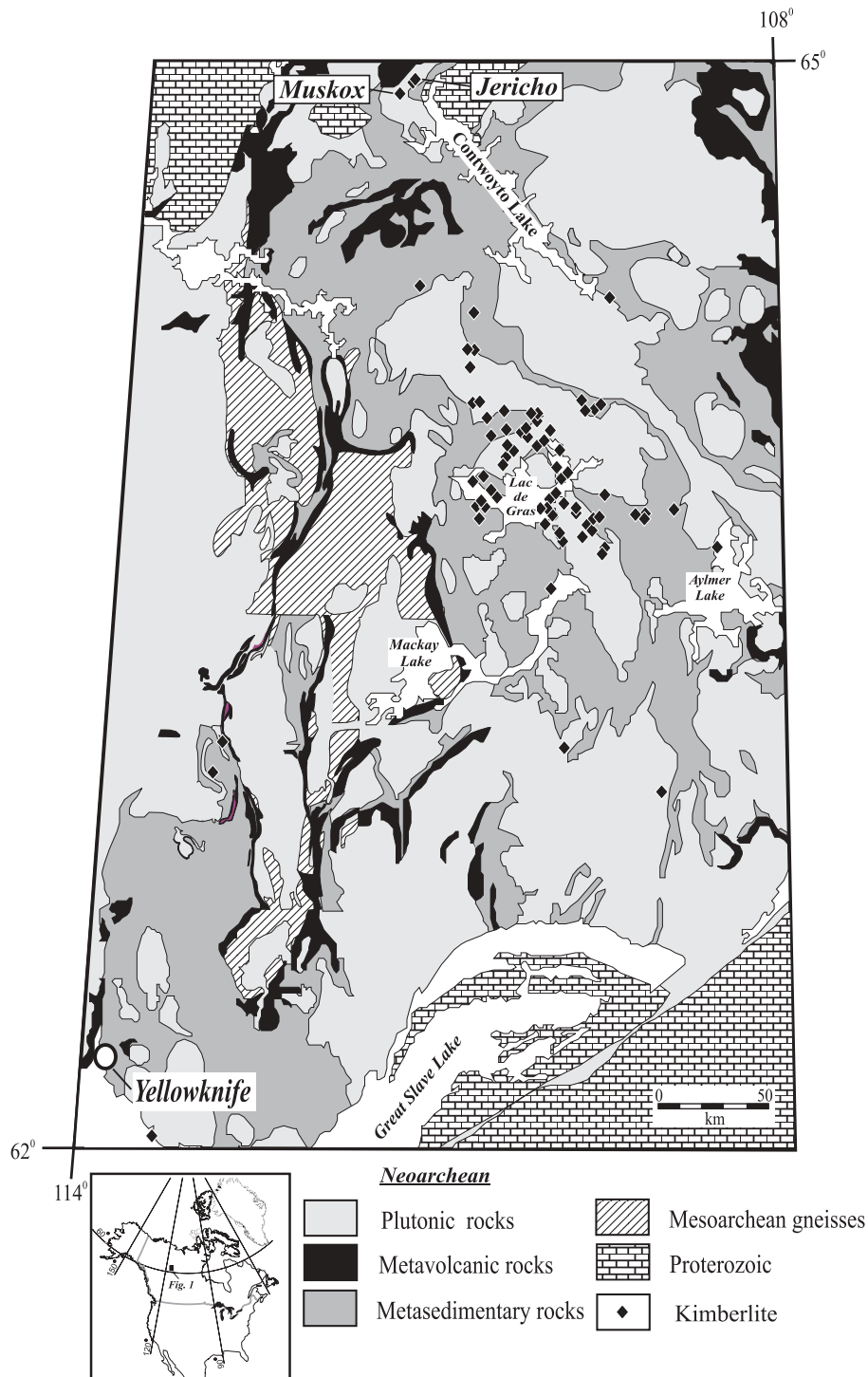
Fig. 1. General geology map of the Slave craton, North America showing the location of kimberlites (♦). The Jericho and Muskox kimberlites are located in the northern Slave Province at the NW end of Contwoyto Lake.

GEOLOGICAL SETTING

The Jericho kimberlites (JD-1, JD-2 and JD-3) are diamondiferous pipes that intrude 2·6 Ga Archean granitoid rocks of the Hackett River Terrane, central Slave craton, Canada. This small kimberlite cluster is located ∼150 km north of the prominent Lac de Gras kimberlite field, and 400 km NE of the city of Yellowknife (Fig. 1). The Jericho kimberlites are located within 10 km and

west of Contwoyto Lake at its northernmost extent. Other kimberlites have been recently discovered in the area (e.g. Muskox, Voyageur and Contwoyto kimberlites; Fig. 1) and all probably belong to a single kimberlite cluster spatially separated from kimberlite pipes near Lac de Gras (Cookenboo, 1998a, 1998b).

The nature of kimberlite magmatism at Jericho has been described in a series of publications reporting the emplacement history (Cookenboo, 1998a, 1998b), petrography and geochemistry (Kopylova et al., 1998a; Price et al., 2000). Most of this research has concentrated on the JD-1 pipe and its northern satellite JD-2. Three distinct types of kimberlite have been recognized at JD-1 and can be distinguished by colour, texture, degree of serpentinization, magnetic susceptibility and density (Cookenboo, 1998a, 1998b). From oldest to youngest the Jericho JD-1 kimberlite phases are: (1) uniform blue–gray to dark gray macrocrystal hypabyssal calcite kimberlite containing macrocrysts of olivine (30 modal %), orthopyroxene, clinopyroxene and ilmenite; (2) dark green pelletal kimberlite consisting of serpentinized olivine macrocrysts and serpentine interclast matrix; (3) greenish gray pelletal kimberlite with macrocrysts of olivine, phlogopite, ilmenite and chrome diopside hosted in a serpentine matrix (Cookenboo, 1998a, 1998b). Kopylova et al. (1998a) concluded that all three phases could be derived from the same parental kimberlite magma based on similarities in trace element contents.

The JD-3 or Nazareth pipe is a steep-walled, pipe-shaped intrusion of elliptical shape (Cookenboo, 1998a). JD-3 is typically fragmental, medium to dark greenish gray, serpentinized and locally carbonatized kimberlite. Two kimberlite textures can be discerned in JD-3: (1) medium greenish gray friable kimberlite that contains abundant large (up to 3 m) limestone xenoliths; (2) dark greenish gray kimberlite with large calcite crystals devoid of large limestone xenoliths. Larger fragments (>1 mm) are consistently rimmed with finely crystalline kimberlite (except for some crustal fragments), and are equivalent to pelletal lapilli of Mitchell (1986) with discrete, rounded margins. Smaller fragments (<0·5 mm) tend to lack such rims. Although extensive alteration makes identification of fragment origin difficult, material of crustal origin (including feldspar, biotite and limestone) can make up ∼15% of the rock and locally JD-3 is a kimberlite breccia. Unaltered olivine is absent but macrocrysts of enstatite and tetraferriphlogopite are common. The presence of larger limestone xenoliths, greater proportion of crustal material, absence of hypabyssal kimberlite and lower density of JD-3 are consistent with a higher stratigraphic position in the Jericho diatreme compared with JD-1.

Mantle xenoliths up to 30 cm in diameter are abundant within Jericho kimberlite and include eclogite (∼25%),

coarse peridotite, porphyroclastic peridotite, megacrystalline pyroxenite and a petrographically distinct suite of ilmenite–garnet wehrlites (Kopylova et al. 1998b; 1999b). subdivided Jericho peridotite xenoliths chemically and texturally into two suites: (1) equilibrated coarse peridotite and spinel/garnet peridotite derived from depths between 45 and 180 km or a low-temperature suite; (2) unequilibrated pyroxenite and porphyroclastic peridotite derived from depths below 190 km or a high-temperature suite. The differences in these xenolith suites were interpreted to indicate the existence of a petrological boundary in the Slave mantle at about 190 km separating lithospheric mantle above the boundary from a more asthenospheric-type mantle below (Kopylova et al., 1998b; Kopylova and Russell, 2000; Kopylova and Caro, 2004).

Based on an examination of 206 eclogite xenoliths from Jericho, Cookenboo et al. (1998a) reported the existence of both massive (∼30%) and foliated varieties. In addition to garnet and omphacite, the Jericho eclogites can contain apatite, ilmenite, rutile and olivine with secondary amphibole, calcite, chlorite, epidote, phlogopite and serpentine (Kopylova et al., 1999a, 2001, 2004; Heaman et al., 2002). In a separate study, Kopylova et al. (2004) investigated the mineralogy of 13 Jericho eclogites and concluded that the primary paragenesis in these xenoliths includes garnet, clinopyroxene, rutile, apatite and sulphide. Two eclogite xenoliths contained ilmenite (no rutile) and one contained trace orthopyroxene. Kopylova et al. interpreted the secondary paragenesis in these xenoliths to include garnet, clinopyroxene, amphibole and phlogopite (interpreted to represent mantle metasomatic minerals) and the alteration minerals serpentine, chlorite and epidote. Rare eclogite types in the Jericho kimberlites include a small proportion of zircon- (2–3%), kyanite-, as well as diamond-bearing eclogite (Cookenboo et al., 1998a; Heaman et al., 2002). The majority of Jericho bimineralic eclogites record paleotemperatures between 800 and 1300°C and, when projected to the 38 mW/m^2 Slave geotherm, are interpreted to be derived from depths between 90 and 195 km (Kopylova et al., 1998b, 1999a, 2001, 2004).

In addition to mantle xenoliths, the pipes in the Jericho kimberlite field entrained a distinctive population of crustal xenoliths, which provide some relative geological constraints on the kimberlite emplacement age, independent of radiometric dates. Most importantly, Middle Devonian (late Eifelian and early Givetian age) limestone xenoliths that were deposited between ∼375 to 385 Ma (Cookenboo et al., 1998b) provide a maximum geological age for the pipe. More tenuously, the lack of wood fragments and Upper Cretaceous to Lower Tertiary mudstones at Jericho, which are common in the pipes near Lac de Gras (Nassichuk & McIntyre, 1995), implies a minimum emplacement age of pre-Late Cretaceous (∼100 Ma).

Table 1: Summary of physical features and mineralogy of Jericho zircon-bearing eclogite xenoliths

Hole		Hole depth	Xenolith	Garnet	Cpx*	Phlog	Rutile	Zircon	Others
1	JDLGS-04		MX1	x	x (<30)			x	
2	JDLGS-09	607′	MX16	x	x (<10)	x	x	x	
3	JDLGS-09	746′	MX17	x	x (>90)		x	x	rutile/zircon composite
4	JDLGS-011	160′ 7″	MX1	x	x (<30)	x	x	x	
5	JDLGS-016		MX12	x	x (<30)			x	
6	JDLGS-017		MX14	x	x (<30)	x			
7	JDLGS-019	174′	MX1	x	x (<10)			x	kyanite
8	JDLGS-019	119′	MX2	x	x (<30)			x	kyanite
9	JDLGS-020	449′	MX4	x	x (<10)	x	x	x	olivine
10	JDLGS-020	622′ 5″	MX7	x	x (50)	x		x	
11	JDLGS-021	335′	MX10	x	x (<10)	x	x	x	calcite, chalcopyrite
12	JDLGS-022	520′ 7″	MX12	x	x (<30)		x	x	kyanite
13	JDLGS-046		MX8	x	x (>90)		x	x	apatite, amphibole
14	JDLGS-056	249′ 6″	MX1 or 2	x	x (>90)	x	x	x	
15	JDLGS-056	847′ 7″	MX3	x	x (>90)	x	x	x	sulphide

*Number in parentheses corresponds to the percentage of clinopyroxene that is altered.

ECLOGITE PETROGRAPHY

Fifteen zircon-bearing and 10 diamond-bearing eclogite xenoliths were made available for this study by Tahera Corporation. A summary of the drill-hole locations and eclogite mineralogy is presented in Table 1. Multiple mantle xenoliths (MX) were recovered in some drill holes and are denoted MX1, MX2, etc. Three zircon-bearing eclogite xenoliths (JDLGS-011 MX1, JDLGS-046 MX8, and JDLGS-021 MX10) were selected for detailed study and the abbreviations MX1, MX8, and MX10 refer to these xenoliths, respectively.

The majority of xenoliths investigated have an interlocking texture of anhedral garnet and clinopyroxene, characteristic of Group II eclogite textures reported elsewhere (e.g. MacGregor & Carter, 1970). Some show evidence of alteration in the form of 0·5–2·0 mm irregular milky white patches (carbonate?) and/or as thin (0·2–2·0 mm) anastomizing grayish green veins dominated by serpentine and chlorite (Fig. 2a). Garnet in all samples has a relatively uniform habit, occurring as large (up to several millimeters) transparent reddish orange crystals devoid of alteration or kelyphite. Alteration veinlets transect garnet crystals and embayment features are common where garnet is in contact with alteration (Fig. 2a). Clinopyroxene is more variable in its petrographic characteristics. In some xenoliths, it occurs as large (up to 5 mm), transparent, unaltered, dark green crystals. In others, the clinopyroxene colour has a much lighter aquamarine hue. Clinopyroxene can be extensively altered to serpentine and one such example

is shown in Fig. 2b (MX10) where only small islands of original clinopyroxene are preserved.

Nine of the xenoliths contain both zircon and rutile (most of these also contain phlogopite) and three contain zircon and kyanite (Table 1). Zircon occurs as euhedral to subhedral large (up to 2 mm), colourless, transparent, multi-faceted prismatic forms (Fig. 2c). It commonly occurs as large inclusions in garnet and in contact with rutile and clinopyroxene, consistent with a metamorphic origin. Zircon is not observed in alteration veins, so we interpret zircon formation to clearly pre-date the latest metasomatic events. Mineral inclusions of ilmenite and garnet were noted in a number of zircon grains. Structural complexity was noted in some crystals using a variety of electron microprobe imaging techniques including elemental X-ray maps (e.g. Hf), backscatter electron and cathodoluminescence (CL) images (Fig. 2c). If the majority of Zr and Hf in the eclogite whole-rock resides in zircon then some xenoliths contain up to 1 modal % zircon.

Rutile occurs as large (up to 2 mm), black crystals with a slightly metallic luster. Thin ilmenite exsolution and linear low-Nb rutile domains occur in most grains (Fig. 2d and e). The Jericho eclogite rutile is most similar in size and texture to the eclogite rutile described from the Stockdale kimberlite, Kansas (Meyer & Boctor, 1975). The main differences are that spinel exsolution and rims of ilmenite are not observed in Jericho rutile. If all Nb in the eclogite whole-rock resides in rutile then some Jericho xenoliths contain up to 3 modal % rutile.
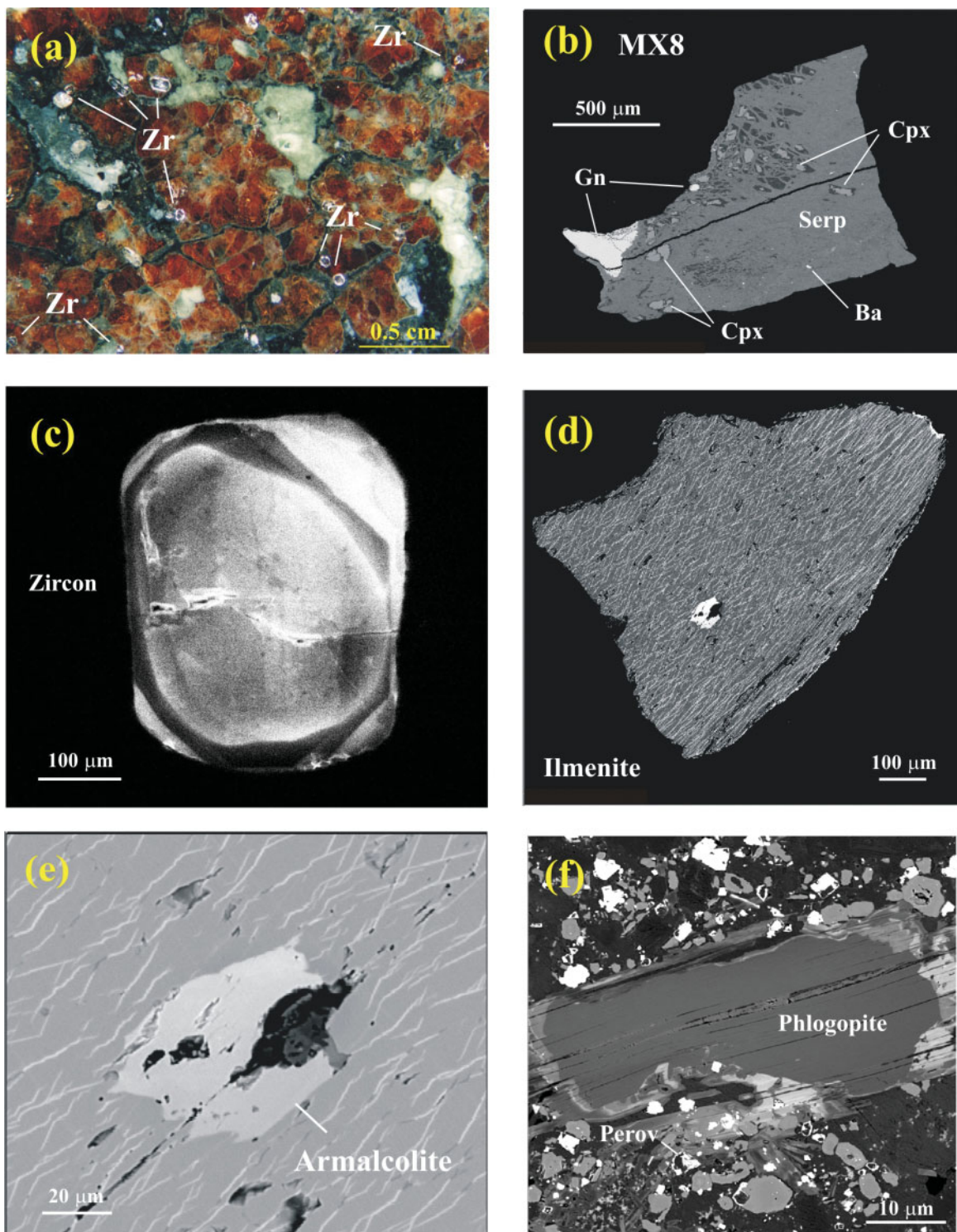
Fig. 2. Photographs of various minerals investigated in this study. (a) General view of a polished slab of eclogite MX1 showing more than 10 zircon crystals. The longest zircon crystal in this photo is 2 mm in length. (b) Backscattered electron image of altered clinopyroxene from eclogite xenolith MX8. Small islands of pristine clinopyroxene are all that remain. (c) Cathodoluminescence image of zircon from eclogite MX8. The zoning, which could reflect multiple periods of zircon growth, should be noted. (d) Backscattered electron image of a rutile crystal from eclogite MX8 containing an armalcolite inclusion. The thin light grey exsolution lamellae are high-Fe rutile and not ilmenite. (e) An expanded view of the armalcolite inclusion. (f) Zoned phlogopite crystal from JD-1 kimberlite. The chemical composition of this grain (rim and core) is reported in Table 3 (JD-1 #1).

In xenolith MX8, rutile is most often associated with the alteration paragenesis but also occurs as inclusions in garnet. The Jericho rutile does not have polycrystalline titanite overgrowth textures, a feature recorded in some massif-type eclogites (e.g. Paquette *et al.*, 1995; Heaman, unpublished mineral data for the Last Peak eclogite reported by Creaser *et al.*, 1997).

Abundant apatite, rutile and zircon were identified in one xenolith, MX8. To our knowledge this xenolith is the first reported kimberlite-borne eclogite xenolith to contain all three accessory minerals. Similar to rutile and zircon, apatite also occurs as relatively large, equant, subhedral crystals (up to 2 mm). Most are transparent and light to dark smoky gray in colour. Some apatite crystals are slightly cloudy, especially in the cores of grains, reflecting the presence of abundant tiny fluid(?) micro-inclusions. These grains have some similarities to apatite reported from metasomatized peridotite xenoliths from Spitsbergen (Ionov *et al.*, 1993). Thin veins of alteration material transect some apatite crystals, indicating that some alteration occurred after apatite crystallization. Trace amounts of amphibole, armalcolite, barite, carbonate, olivine and sulphide are present in some xenoliths.

MINERAL CHEMISTRY

The mineral analyses were obtained using a JEOL8900 electron probe microanalyzer, operated at 15 kV accelerating voltage and 15 nA beam current, at the University of Alberta. Natural garnet, and clinopyroxene standards from the Smithsonian Institution (Jarosewich, 2002) and several synthetic materials were used for standardization. The data for MX1, Zr1-6 and garnet from all diamond-bearing eclogites were determined using a CAMECA SX50 electron microprobe at the University of British Columbia [for analytical protocols see Kopylova *et al.* (1999*a*)].

Garnet

The average compositions of garnet from nine Jericho zircon-bearing eclogites and 10 diamond-bearing eclogites are reported in Table 2. In general, the garnet chemistry within individual eclogite xenoliths is relatively homogeneous. Traverses comprising 10–19 spot analyses per grain were conducted for several grains from xenoliths MX8 and MX10 and these grains show no evidence of chemical zoning. The zircon-bearing eclogitic garnets generally have a uniform composition with high FeO (22·6–27·5 wt %) and low MgO (4·0–7·6 wt %; filled squares in Fig. 3a), whereas the diamond-bearing eclogitic garnets (filled diamonds in Fig. 3a) have high MgO (19·6–21·3 wt %), low FeO (8·7–11·5 wt %), and low, relatively uniform CaO contents (4·1–4·3 wt %). The zircon- and diamond-bearing eclogitic garnets have

distinctly different compositions compared with all other eclogitic garnet previously reported from Jericho (e.g. see Fig. 3a; Kopylova *et al.*, 1999*a*, 2004). Garnet from one zircon-bearing eclogite (Zr3) has a much higher CaO and lower FeO content compared with other similar xenoliths (Fig. 3a). Based on the Na_2O content in garnet classification scheme of McCandless & Gurney (1989), the majority of Jericho eclogitic garnets would be classified as Group II (i.e. having <0·09 wt % Na_2O). Interestingly, eclogite xenolith MX10 does show some variation in garnet composition (0·06–0·31 wt % Na_2O). Four of the five grains analysed have Na_2O contents similar to garnet from all other Jericho eclogite xenoliths (0·06–0·11 wt %). The exception is one high-Na_2O garnet grain (0·31 wt %) that is more akin to a Group I eclogite (McCandless & Gurney, 1989) and is characteristic of eclogitic garnet inclusions in diamond from elsewhere (e.g. Stachel *et al.*, 2000). However, this high Na_2O content does not correlate with higher MgO contents that are more typical for garnet from diamond-bearing eclogite.

Clinopyroxene

The chemical composition of clinopyroxene from two zircon-bearing and seven diamond-bearing eclogite xenoliths are presented in Table 2 and on a MgO–Na_2O variation diagram in Fig. 3b. Also shown for reference in Fig. 3b are the boundaries separating the various fields for Groups A–C eclogite (Coleman *et al.*, 1965; Shervais *et al.*, 1988). In some Jericho eclogite xenoliths, the clinopyroxene is extensively altered to serpentine, so obtaining primary chemical data can be challenging. One such example is the clinopyroxene in MX8, which is >90% altered to serpentine and only tiny islands of pristine clinopyroxene remain (Fig. 2b). Despite this extensive alteration, the pyroxene islands in MX8 have a relatively homogeneous composition both within individual islands (the data in Table 2 represent an average of 7–10 spot analyses) and between islands within the same grain. In contrast, the clinopyroxene in eclogite xenolith MX10 is fresh with only traces of alteration. The average chemical compositions of clinopyroxene in both zircon-bearing xenoliths are similar (Table 2) and plot in the Group C field in Fig. 3b (filled squares). The high Na_2O and Al_2O_3 combined with the low MgO and CaO contents of clinopyroxene from the zircon-bearing eclogites lie in stark contrast to clinopyroxene from Jericho diamond-bearing eclogites (filled diamonds; Fig. 3b), which have some of the lowest Na_2O (0·44–1·50 wt %) and Al_2O_3 (1·96–2·89 wt %) contents with some of the highest CaO (20·49–23·49 wt %) contents reported for clinopyroxene from any kimberlite-borne eclogite xenolith, plotting within the Group A field in Fig. 3b (filled diamonds). Similar to the garnet results presented above, clinopyroxene from the diamond-bearing and

Table 2: Mineral chemistry for Jericho eclogite xenoliths: garnet and clinopyroxene

Zircon-bearing eclogite

	MX1	MX8	MX8	MX10	MX10	Zr1*	Zr2*	Zr3*	Zr4*	Zr5*	Zr6*
	Gnt	Gnt	Cpx	Gnt	Cpx	Gnt	Gnt	Gnt	Gnt	Gnt	Gnt
n:	2	5	3	6	5	1	1	1	1	1	1
SiO_2	37.71	37.79 (0.07)	56.41 (0.10)	37.62 (0.06)	56.24 (0.14)	37.45	37.38	38.30	37.13	37.21	38.17
TiO_2	0.26	0.07 (0.01)	0.13 (0.01)	0.10 (0.02)	0.14 (0.02)	0.08	0.11	0.15	0.13	0.09	0.11
Al_2O_3	21.56	21.77 (0.06)	14.33 (0.01)	21.57 (0.12)	13.12 (0.16)	21.60	21.53	22.18	21.45	21.45	22.10
Cr_2O_3	0.05	0.01 (0.01)	0.01 (0.01)	0.01 (0.01)	0.01 (0.01)	b.d.	0.03	b.d.	0.01	0.01	0.05
FeO	23.04	26.26 (0.04)	6.61 (0.07)	26.54 (0.82)	6.97 (0.05)	26.15	27.20	17.94	26.74	27.47	22.99
MgO	5.79	4.73 (0.10)	4.98 (0.04)	4.10 (0.24)	5.64 (0.11)	4.26	4.15	4.25	4.14	4.01	7.57
MnO	0.28	0.66 (0.03)	0.03 (0.01)	0.76 (0.05)	0.04 (0.01)	b.d.	b.d.	b.d.	b.d.	b.d.	b.d.
CaO	11.11	8.66 (0.16)	8.57 (0.02)	9.02 (0.28)	9.72 (0.13)	9.88	9.13	17.07	9.42	9.39	8.91
Na_2O	0.05	0.06 (0.01)	9.33 (0.09)	0.12 (0.09)	8.55 (0.05)	0.05	0.04	0.06	0.04	0.07	0.05
Total	99.81	100.02 (0.16)	100.41 (0.21)	99.83 (0.27)	100.42 (0.26)	100.49	100.35	100.29	99.06	100.50	100.50
Si	2.939	2.962	1.996	2.965	1.998	2.956	2.955	2.952	2.950	2.946	2.941
Ti	0.015	0.004	0.003	0.006	0.004	0.005	0.007	0.009	0.008	0.005	0.006
Al	1.975	2.011	0.598	2.004	0.549	2.009	2.006	2.014	2.008	2.001	2.007
Cr	0.003	0.001	0.000	0.001	0.000	0.000	0.002	0.000	0.001	0.001	0.003
Fe	1.462	1.721	0.195	1.749	0.207	1.726	1.798	1.156	1.776	1.819	1.481
Mg	0.827	0.552	0.263	0.481	0.299	0.501	0.489	0.488	0.490	0.473	0.870
Mn	0.027	0.044	0.001	0.051	0.001	0.000	0.000	0.000	0.000	0.000	0.000
Ca	0.805	0.728	0.325	0.761	0.370	0.835	0.773	1.409	0.802	0.796	0.736
Na	0.010	0.010	0.640	0.019	0.589	0.008	0.006	0.009	0.006	0.011	0.007
Sum	8.062	8.033	4.022	8.036	4.018	8.039	8.037	8.037	8.041	8.053	8.051
$T(°C)^1$			1019	948							
$T(°C)^2$			1091	1000							

Diamond-bearing eclogite

	135-F*	135-F*	135-F*	135-F*	135-F*	135-F*	135-F*	135-F*	135-F*	135-F*	135-G*	135-G*	131*	123-F*	123-F*	132*	109*
	Ecl#1	Ecl#1	Ecl#3	Ecl#3	Ecl#4	Ecl#4	Ecl#5	Ecl#5	Ecl#6	Ecl#6	Ecl#7	Ecl#7					
	Gnt	Cpx	Gnt	Cpx	Gnt	Cpx	Gnt	Cpx	Gnt	Cpx	Gnt	Cpx	Gnt	Gnt	Cpx	Gnt	Gnt
n:	2	2	3	2	2	2	1	2	1	2	2	3	3	6	4	2	5
SiO_2	41.10	53.53	41.20 (0.46)	54.22	40.78	53.58	40.66	54.07	41.22	53.31	40.98	53.65 (0.10)	40.98 (0.16)	41.20 (0.22)	54.19 (0.32)	41.42	40.90 (0.24)
TiO_2	0.25	0.12	0.1 (0.02)	0.11	0.22	0.14	0.20	0.16	0.22	0.18	0.21	0.18 (0.01)	0.22 (0.05)	0.20 (0.02)	0.16 (0.01)	0.20	0.15 (0.16)
Al_2O_3	23.68	2.09	23.71 (0.07)	2.82	23.54	2.21	23.44	2.59	23.44	2.24	23.57	2.30 (0.13)	23.47 (0.09)	23.30 (0.09)	2.10 (0.04)	23.55	23.27 (0.11)
Cr_2O_3	0.34	0.15	0.52 (0.08)	0.24	0.45	0.11	0.33	0.17	0.28	0.14	0.40	0.21 (0.03)	0.33 (0.06)	0.39 (0.02)	0.30 (0.09)	0.45	0.29 (0.04)
FeO	10.67	2.75	8.75 (0.06)	2.27	10.41	2.82	10.35	2.68	11.45	3.20	10.29	2.78 (0.08)	10.10 (0.14)	9.97 (0.19)	2.69 (0.12)	10.21	10.91 (0.18)
MgO	20.16	16.97	21.19 (0.01)	16.58	20.36	16.88	20.22	16.63	19.56	16.68	20.35	16.72 (0.06)	19.92 (0.04)	20.12 (0.05)	16.98 (0.09)	20.05	19.60 (0.02)
MnO	0.46	0.08	0.41 (0.06)	0.07	0.38	0.14	0.41	0.07	0.37	0.08	0.41	0.09 (0.05)	0.38 (0.07)	0.36 (0.12)	0.06 (0.01)	0.37	0.38 (0.11)
CaO	4.21	21.14	4.16 (0.10)	20.85	4.16	21.01	4.07	20.78	4.14	20.70	4.07	20.64 (0.19)	4.13 (0.01)	4.09 (0.05)	20.84 (0.16)	4.14	4.06 (0.04)
Na_2O	0.04	1.13	0.04 (0.01)	1.38	0.03	1.18	0.03	1.28	0.04	1.20	0.05	1.23 (0.06)	0.05 (0.01)	0.05 (0.01)	1.49 (0.03)	0.04	0.05 (0.01)
Total	100.91	97.97	100.15 (0.73)	98.55	100.32	98.07	99.69	98.43	100.73	97.73	100.30	97.79 (0.27)	99.58 (0.12)	99.68 (0.26)	98.82 (0.42)	100.42	99.61 (0.34)
Si	2.923	1.976	2.926	1.981	2.915	1.976	2.922	1.981	2.943	1.975	2.926	1.981	2.943	2.953	1.982	2.950	2.946
Ti	0.013	0.003	0.009	0.003	0.012	0.004	0.011	0.004	0.012	0.005	0.011	0.005	0.012	0.011	0.004	0.011	0.008
Al	1.984	0.091	1.985	0.122	1.983	0.096	1.985	0.112	1.972	0.098	1.983	0.100	1.986	1.968	0.091	1.976	1.976
Cr	0.019	0.005	0.029	0.007	0.025	0.003	0.019	0.005	0.016	0.004	0.023	0.006	0.019	0.022	0.009	0.025	0.017
Fe	0.634	0.085	0.519	0.069	0.622	0.087	0.622	0.082	0.684	0.099	0.614	0.086	0.607	0.598	0.082	0.608	0.657
Mg	2.137	0.934	2.244	0.903	2.169	0.928	2.166	0.909	2.082	0.921	2.165	0.921	2.133	2.150	0.926	2.129	2.105
Mn	0.028	0.003	0.025	0.002	0.023	0.002	0.025	0.002	0.022	0.003	0.024	0.003	0.023	0.022	0.002	0.022	0.023
Ca	0.321	0.836	0.317	0.816	0.319	0.830	0.313	0.816	0.317	0.821	0.311	0.816	0.318	0.314	0.817	0.316	0.313
Na	0.005	0.081	0.005	0.098	0.005	0.085	0.004	0.091	0.005	0.086	0.007	0.088	0.006	0.007	0.105	0.006	0.007
Sum	8.065	4.013	8.060	4.001	8.072	4.012	8.067	4.002	8.053	4.012	8.064	4.005	8.046	8.045	4.017	8.042	8.053
$T(°C)^1$	989		1019		1028		996		1015		1015			1003			
$T(°C)^2$	949		983		996		956		981		960			963			

$T(°C)^1$ Ellis & Green (1979); $T(°C)^2$ Krogh-Ravna (2000). Temperatures calculated based on $P = 50$ kbar. Cation proportions based on 12 (garnet) and six (clinopyroxene) oxygen atoms. Numbers in parentheses are standard deviations for samples where three or more mineral grains were analysed. *Analyses conducted at the University of British Columbia using a CAMECA SX50 electron microprobe (b.d., below detection limit).
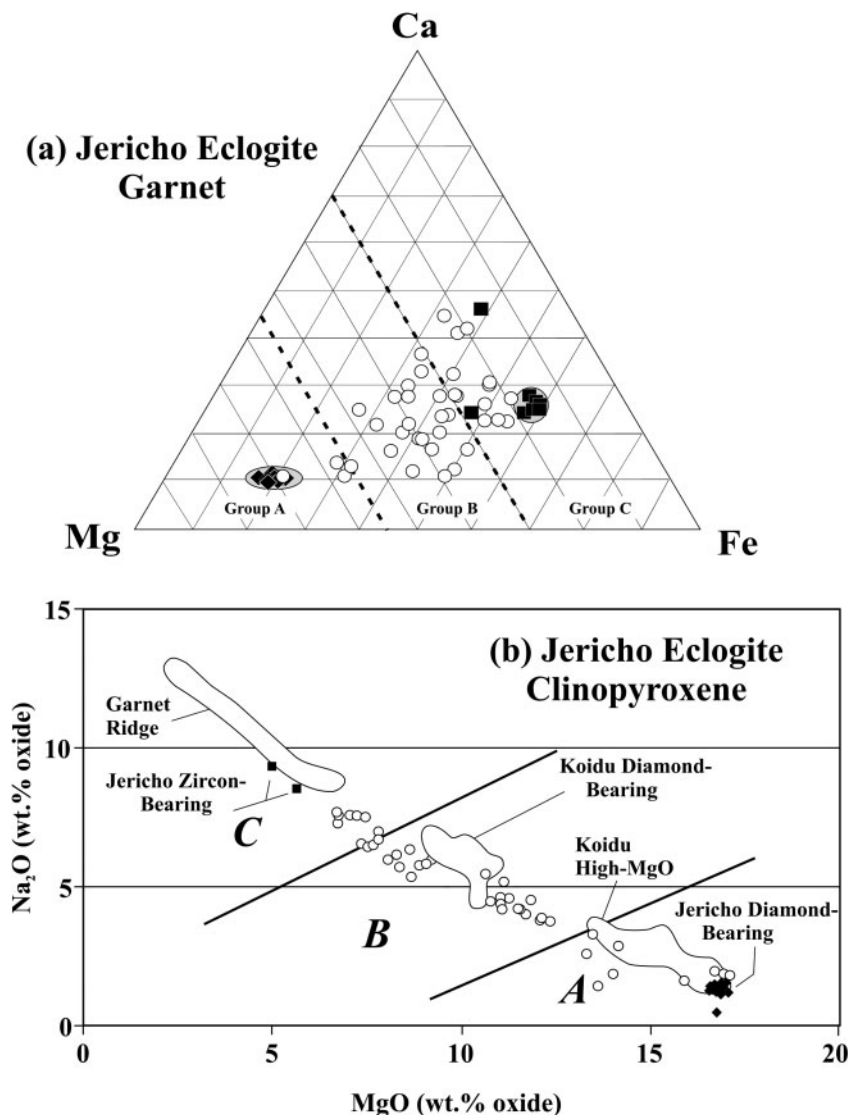
Fig. 3. (a) Ternary plot showing garnet composition from Jericho eclogite xenoliths. The fields for garnet isolated from Group A-C eclogites [defined by Coleman *et al.* (1965)] are also shown. The data are divided into zircon-bearing (■), diamond-bearing (♦) and all other eclogite types (○) reported by Kopylova *et al.* (1999*a*, 2004). The garnets from diamond-bearing and zircon-bearing eclogites, respectively cluster at the high-Mg and high-Fe extremes of the typical eclogitic garnet range. (b) Na_2O vs MgO (weight per cent oxide) plot for clinopyroxene from Jericho eclogites. Symbols are the same as in (a). The fields for clinopyroxene isolated from Group A–C eclogites [defined by Coleman *et al.* (1965)] are also shown. For comparison, the fields for clinopyroxene from Garnet Ridge, and Koidu, Sierra Leone, diamond-bearing and high-MgO eclogites (Hills & Haggerty, 1989) are shown. Also plotted are the compositions of a variety of eclogite clinopyroxenes (○) previously reported from Jericho (Kopylova *et al.*, 1999*a*, 2004).

zircon-bearing eclogites plots at opposite ends of the compositional range reported for Jericho eclogitic clinopyroxene (Kopylova *et al.*, 1999*a*, 2004; Fig. 3b).

Phlogopite

The average compositions of two phlogopite crystals from one zircon-bearing eclogite xenolith (MX10) are reported in Table 3 and represent traverses consisting of 12–14 spot analyses per grain conducted across basal sections. These phlogopite grains have relatively uniform compositions, both within and between grains. For example, MX10 grain #1 shows only minor within-grain chemical variation with little evidence for compositional zoning. MX10 #2 phlogopite shows slight compositional zoning with a small core region containing more FeO (up to 12·63 wt %) and less MgO (16·66 wt %). It is possible that the high TiO_2 content of MX10 phlogopite (4·17–4·48 wt %) could reflect high-temperature equilibration with a high-Ti phase such as rutile.

Table 3: Mineral chemistry for Jericho eclogite xenoliths: phlogopite and apatite

	Phlogopite—eclogite		Phlogopite—kimberlite					
	MX10	MX10	JD-1	JD-1	JD-1	JD-1	JD-1	JD-1
	#1	#2	#1 rim	#1 core	#2	#3 rim	#3 core	#4
n:	12	14	15	13	10	2	8	9
SiO_2	38·67 (0·78)	40·31 (0·89)	36·59 (2·04)	42·47 (0·20)	36·15 (0·88)	40·19	36·04 (2·48)	36·92 (0·75)
TiO_2	4·17 (0·15)	4·48 (0·16)	1·48 (0·22)	0·19 (0·06)	0·93 (0·35)	0·43	1·29 (0·57)	1·04 (0·24)
Al_2O_3	15·30 (0·27)	14·79 (0·66)	14·62 (1·82)	10·38 (0·32)	17·12 (0·43)	4·80	16·47 (1·24)	16·97 (0·25)
Cr_2O_3	—	—	—	—	—	—	—	—
FeO	8·57 (0·13)	6·42 (0·39)	2·63 (0·57)	3·88 (0·09)	2·84 (0·11)	7·44	2·80 (0·15)	2·81 (0·19)
MgO	18·19 (0·30)	19·15 (0·48)	25·46 (1·42)	26·82 (0·37)	24·91 (0·54)	28·13	24·99 (1·01)	25·35 (0·28)
MnO	0·04 (0·01)	0·04 (0·03)	0·04 (0·01)	0·02 (0·01)	0·05 (0·03)	0·06	0·03 (0·01)	0·03 (0·01)
CaO	0·01 (0·01)	0·01 (0·02)	0·04 (0·19)	0·03 (0·03)	0·07 (0·08)	1·65	0·24 (0·36)	0·06 (0·07)
Na_2O	0·52 (0·08)	0·44 (0·09)	0·03 (0·02)	0·14 (0·03)	0·03 (0·03)	0·22	0·10 (0·07)	0·02 (0·03)
K_2O	9·67 (0·44)	9·76 (0·36)	8·32 (0·96)	10·51 (0·40)	9·79 (0·76)	9·26	8·86 (1·29)	9·84 (0·51)
BaO	0·24 (0·05)	0·15 (0·05)	5·86 (2·54)	0·91 (0·23)	3·66 (2·21)	0·62	5·25 (3·43)	3·35 (1·67)
F	0·22 (0·04)	0·27 (0·07)	1·06 (0·26)	0·51 (0·05)	0·44 (0·13)	0·30	0·58 (0·35)	0·49 (0·13)
Cl	0·08 (0·02)	0·08 (0·02)	0·02 (0·03)	0·02 (0·02)	0·01 (0·01)	0·38	0·09 (·014)	0·01 (0·01)
Total	95·57 (0·99)	96·07 (0·66)	95·91 (1·50)	95·88 (0·45)	96·29 (1·69)	93·48	96·11 (2·48)	96·67 (0·72)

	Apatite				
	MX8	MX8	MX8	MX8	MX8
	#1	#2	#3	#4	#5
n:	20	20	5	20	20
SiO_2	0·01 (0·03)	b.d.	b.d.	b.d.	b.d.
Al_2O_3	0·01 (0·01)	0·01 (0·04)	b.d.	0·01 (0·02)	b.d.
FeO	0·34 (0·12)	0·41 (0·04)	0·40 (0·02)	0·40 (0·04)	0·38 (0·02)
MgO	0·12 (0·05)	0·15 (0·03)	0·14 (0·02)	0·14 (0·02)	0·14 (0·02)
CaO	52·56 (0·97)	51·35 (0·75)	51·24 (0·53)	50·59 (0·36)	50·82 (0·30)
Na_2O	0·17 (0·05)	0·19 (0·06)	0·15 (0·05)	0·16 (0·04)	0·16 (0·04)
P_2O_5	40·02 (0·70)	38·31 (0·75)	37·56 (1·25)	36·38 (0·68)	37·37 (0·68)
F	3·32 (0·15)	3·48 (0·15)	3·32 (0·08)	3·60 (0·14)	3·59 (0·14)
Cl	0·32 (0·09)	0·31 (0·03)	0·30 (0·02)	0·30 (0·03)	0·34 (0·03)
SrO	0·85 (0·35)	0·89 (0·08)	0·92 (0·07)	0·81 (0·09)	0·85 (0·08)
La_2O_3	0·31 (0·07)	0·25 (0·06)	0·25 (0·06)	0·29 (0·05)	0·26 (0·05)
Ce_2O_3	0·85 (0·06)	0·6 (0·05)	0·60 (0·03)	0·61 (0·05)	0·60 (0·05)
Nd_2O_3	0·24 (0·06)	0·25 (0·06)	0·20 (0·06)	0·26 (0·05)	0·26 (0·04)
Total	97·40 (0·85)	94·65 (1·28)	93·69 (1·80)	91·96 (0·81)	93·18 (0·89)

Data obtained using JEOL8900 electron microprobe at the University of Alberta. Numbers in parentheses represent standard deviations for multiple analyses per grain.

Compared with phlogopite from Koidu eclogites (Hills & Haggerty, 1989), the Jericho MX10 phlogopite is compositionally similar, with the exception of slightly higher TiO_2 contents (Koidu eclogite phlogopites have between 1·58 and 4·00 wt % TiO_2).

For comparison, the chemical compositions for four phlogopite grains in the host JD-1 kimberlite are reported in Table 3. Many of the kimberlitic phlogopite grains exhibit pronounced zoning when viewed with back-scatter imaging (Fig. 3f). It is interesting that the zoning

patterns are not consistent. For example, the rim on JD-1 grain #1 is enriched in TiO_2, Al_2O_3, CaO, and BaO (see Table 3), whereas in grain #3 it is the reverse. In general, the Jericho kimberlitic phlogopite is chemically distinct from the eclogitic phlogopite in having lower TiO_2 and FeO, and much higher BaO. In addition, eclogite MX10 phlogopite has considerably lower MgO contents (18·2 wt % compared with a range of 25·0–28·1 wt % for the kimberlite phlogopite).

Apatite

One eclogite xenolith in this study (MX8) contains abundant, relatively large, discrete crystals of gray fluorapatite (3·3–3·6 wt % F). The average chemical compositions for five apatite grains are presented in Table 3. Fluorapatite in this eclogite is chemically similar to Type B mantle apatite reported by O'Reilly & Griffin (2000), and to apatite in carbonatites in general (e.g. Hogarth, 1989). The low uranium contents (11 ppm) and Th/U (1·8–1·9) reported in Table 7 are also geochemical features consistent with Type B mantle fluorapatite (O'Reilly & Griffin, 2000).

Rutile and armalcolite

The chemical compositions of four rutile grains from xenolith MX8 and five rutile grains from MX10 are presented in Table 4. The Jericho rutile compositions are compared with rutile from other eclogite (open squares and triangles) and peridotite (open circles) xenoliths in Fig. 4a and b. Other unusual xenolith types that are represented in Fig. 4a include kyanite eclogites or corundum eclogites (i.e. peraluminous; open triangles), two unusual high-SiO_2 eclogite xenoliths from Moses Rock (shaded square), and two LIMA (lindsleyite- and mathiasite-bearing) xenoliths (filled circles). Rutiles from a variety of ultramafic xenoliths [lherzolite, harzburgite, LIMA, MARID (mica–amphibole–rutile–ilmenite–diopside)] display a high-Cr_2O_3 trend (denoted peridotite trend in Fig. 4a and b) with some of the most chromian rutiles (up to 7·2 wt % Cr_2O_3 in this diagram) occurring in peridotite and LIMA xenoliths entrained in Bultfontein and Jagersfontein kimberlites, respectively (Smith & Dawson, 1975; Dawson & Smith, 1977; Haggerty, 1983). Rutiles with nearly 10 wt % Cr_2O_3 are reported from armalcolite-bearing xenoliths from Jagersfontein (Haggerty, 1983). The high-chromium rutile signature from ultramafic xenoliths presumably reflects the ambient high-Cr nature of the mantle material from which they formed.

The composition of rutile from Jericho zircon-bearing eclogites is unusual with respect to both its high Al_2O_3 (0·57–1·05 wt %) and Nb_2O_5 (4·32–5·76 wt %) contents (Fig. 4a and b). Their high Al_2O_3 contents are similar to rutile compositions in peraluminous eclogite and hint at a high-Al protolith for these eclogites. Rutiles

from other xenoliths, such as those from the LIMA inclusions entrained in Jagersfontein kimberlite (Haggerty, 1983), can have much higher Nb_2O_5 contents (up to 21 wt % in the Nb–Cr rutiles from Orapa; Tollo & Haggerty, 1987) but have the low Al_2O_3 signature of ultramafic xenoliths. From our literature search, only one other eclogite xenolith shows this dual high-Al and high-Nb character, sample 81-21 from Koidu (Hills & Haggerty, 1989).

When viewed with BSE imaging (e.g. Fig. 2d), all Jericho eclogite rutile contain bright 1–2 μm wide lamellae that have a regular spacing of ∼10 μm. These lamellae often form a trellis pattern and are very similar to textures described for mantle rutile from the Stockdale kimberlite, Kansas (Meyer & Boctor, 1975), interpreted as ilmenite exsolution lamellae. Although the Jericho rutile lamellae are so narrow that quantitative EMP analyses are challenging, the chemical data for 6–9 lamellae from four rutile grains in MX10 (Table 4) indicate that either these lamellae are high-Fe rutile and not ilmenite (as in other mantle rutile examples) or more probably the data indicate a mixed rutile plus ilmenite analysis. In addition to these lamellae, occasional tiny ilmenite inclusions do occur. In one MX10 rutile grain the ilmenite inclusion is corroded and embayed.

An exciting result from this study was the discovery of an ∼40 μm armalcolite $(Fe,Mg)Ti_2O_5$ inclusion in a rutile grain from MX8 (see Fig. 2d and e). Armalcolite could form within rutile during decompression if rutile were to react with ilmenite exsolution lamellae, but the high CaO content of the Jericho MX8 armalcolite (Table 4) indicates that this is probably not the case (i.e. would require an external source for Ca). The discovery of this inclusion has great importance because the growth of armalcolite is generally linked to metasomatism in the upper mantle (e.g. Haggerty, 1992). The average chemical composition based on 11 spot analyses is presented in Table 4. The low totals for the armalcolite analysis could reflect the presence of some zirconium as Cr–Ca(NbZr) armalcolites can contain up to 3 wt % ZrO_2 (Haggerty, 1992) or possibly K_2O as noted in Argyle armalcolites (Jaques *et al.*, 1989). In some respects this armalcolite inclusion has an intermediate composition with some chemical features akin to Cr–Ca(NbZr) armalcolites (high Nb_2O_5, CaO and SrO of 2·44, 2·67 and 0·99 wt %, respectively), Cr-armalcolite (high MgO + FeO >20 wt %) and Zr-armalcolite (i.e. very low Cr_2O_3). However, it does not readily fit into the chemical classification scheme of Haggerty (1992).

Zircon

Zircon crystals isolated from Jericho eclogites generally have low uranium (9–62 ppm), low thorium (1–13 ppm) and low Th/U (0·05–0·37). These results are somewhat similar to the zircon compositions (4–13 ppm, 1–2 ppm

Table 4: Mineral chemistry for Jericho eclogite xenoliths: oxide minerals

	MX8					MX10									
	Rutile	Rutile	Rutile	Rutile	Armacolite*	Rutile	Rutile	Rutile	Rutile	Rutile	Ilmenite*	Fe-rutile	Fe-rutile	Fe-rutile	Fe-rutile
	Grain 1	Grain 2	Grain 3	Grain 4	Grain 1	Grain 1	Grain 2	Grain 3	Grain 4	Grain 5	Grain 2	Grain 2	Grain 3	Grain 4	Grain 5
n:	10	12	11	9	11	10	10	13	19	15	2	6	8	9	9
TiO_2	91·42 (0·11)	91·47 (0·39)	90·99 (0·31)	91·22 (0·31)	65·74 (2·43)	89·72 (0·58)	89·84 (0·31)	91·17 (0·32)	91·37 (0·39)	92·49 (0·53)	47·35 (0·72)	83·04 (0·86)	81·56 (1·89)	79·99 (3·26)	81·56 (3·94)
Al_2O_3	0·94 (0·03)	0·97 (0·04)	0·83 (0·05)	0·87 (0·03)	3·51 (0·19)	0·60 (0·13)	0·69 (0·06)	0·61 (0·05)	1·02 (0·08)	0·76 (0·10)	0·64 (0·01)	0·88 (0·33)	0·72 (0·03)	0·91 (0·13)	0·68 (0·07)
Cr_2O_3	0·01 (0·01)	0·01 (0·02)	0·01 (0·01)	0·01 (0·01)	0·01 (0·02)	0·01 (0·01)	0·01 (0·02)	0·01 (0·01)	0·01 (0·02)	0·03 (0·04)	0·01 (0·02)	0·02 (0·02)	0·01 (0·01)	0·01 (0·01)	0·01 (0·01)
FeO	1·65 (0·05)	1·48 (0·06)	2·18 (0·08)	1·80 (0·04)	19·64 (1·39)	3·05 (0·10)	2·89 (0·05)	2·57 (0·08)	1·64 (0·25)	2·33 (0·19)	46·51 (0·47)	10·25 (1·24)	12·11 (2·10)	15·11 (2·62)	15·59 (3·25)
MgO	0·01 (0·01)	0·01 (0·01)	0·01 (0·01)	0·01 (0·01)	0·60 (0·18)	0·01 (0·01)	0·01 (0·02)	0·01 (0·01)	0·01 (0·01)	0·01 (0·01)	0·97 (0·03)	0·23 (0·06)	0·26 (0·03)	0·60 (0·23)	0·33 (0·09)
MnO	0·01 (0·01)	0·01 (0·01)	0·01 (0·01)	0·01 (0·01)	0·04 (0·03)	0·01 (0·01)	0·01 (0·01)	0·01 (0·01)	0·01 (0·01)	0·01(0·01)	0·08 (0·01)	0·01 (0·01)	0·01 (0·01)	0·23 (0·11)	0·01 (0·02)
CaO					2·67 (0·53)										
SrO					1·49 (0·47)										
V_2O_5	0·21 (0·05)	0·23 (0·12)	0·25 (0·08)	0·44 (0·08)	0·57 (0·03)	0·82 (0·02)	0·83 (0·03)	0·85 (0·03)	0·80 (0·02)	0·76 (0·02)	0·47 (0·01)	0·79 (0·03)	0·80 (0·04)	0·69 (0·05)	0·66 (0·02)
Nb_2O_5	5·66 (0·12)	5·76 (0·14)	5·71 (0·14)	5·61 (0·05)	2·44 (0·14)	4·80 (0·22)	4·84 (0·22)	4·32 (0·15)	5·18 (0·10)	4·54 (0·15)	0·50 (0·02)	4·45 (0·32)	4·20 (0·15)	4·76 (0·20)	4·07 (0·18)
Ta_2O_5	0·04 (0·05)	0·04 (0·05)	0·05 (0·06)	0·03 (0·03)											
Total	99·96 (0·11)	99·99 (0·32)	99·99 (0·43)	99·98 (0·39)	96·21 (1·04)	99·01 (0·27)	99·19 (0·29)	99·50 (0·21)	99·96 (0·26)	100·91 (0·22)	98·75 (0·36)	99·50 (0·21)	100·15 (0·30)	100·79 (0·61)	101·37 (0·44)

Data obtained using the University of Alberta JEOL8900 electron microprobe. Numbers in parentheses represent standard deviations for multiple spot analyses per grain. *n*, number of spot analyses per grain.
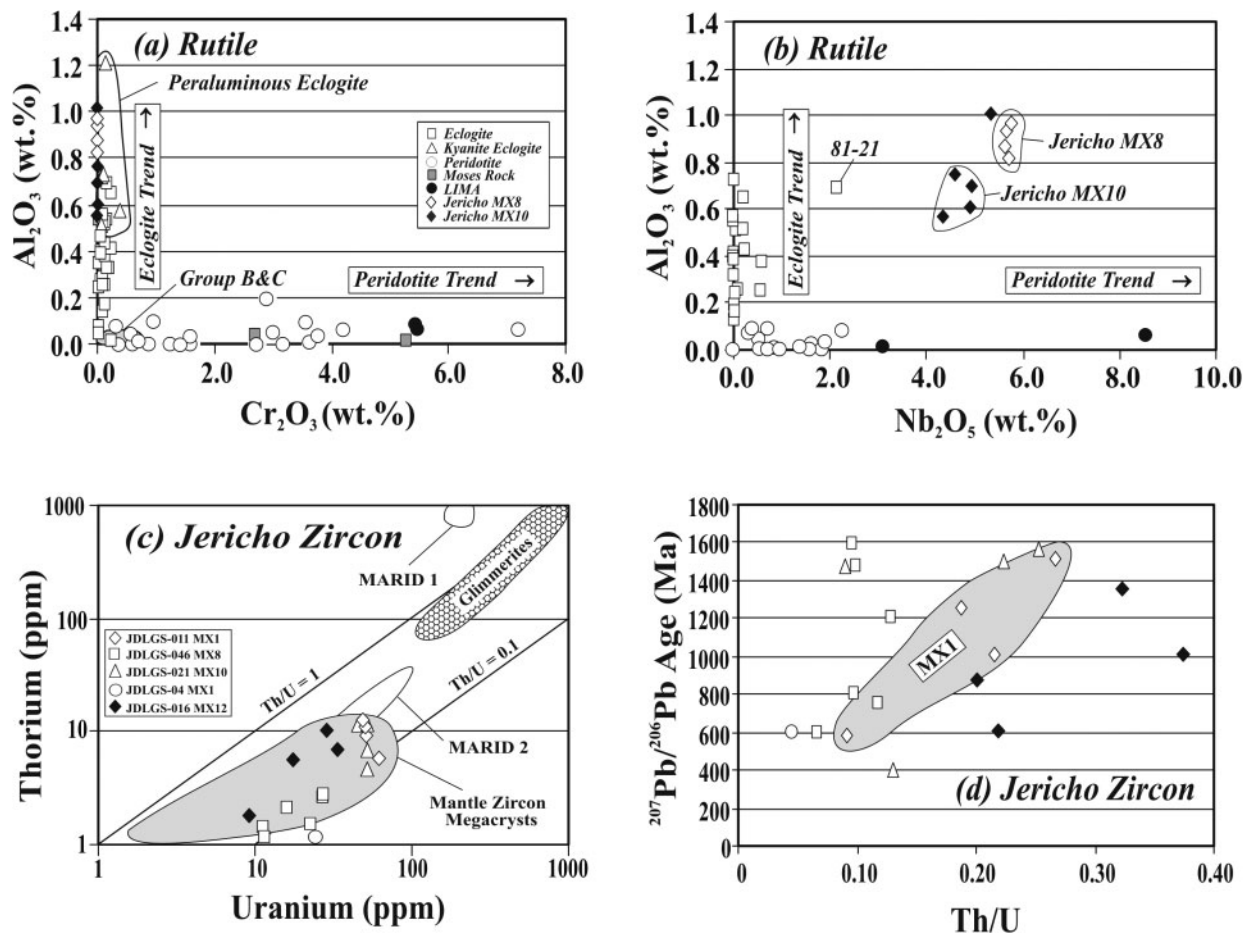*Mineral inclusions.

Fig. 4. Mineral chemistry for Jericho rutile and zircon. (a) Al_2O_3 vs Cr_2O_3, demonstrating the low-Cr/high-Al nature of Jericho rutile compared with other eclogitic rutile. (b) Al_2O_3 vs Nb_2O_5, illustrating the unique chemical characteristics of Jericho eclogite rutile compared with rutile analysed from all other cratonic eclogites. Symbols are the same as in (a). (c) Th vs U concentration in Jericho eclogite zircon. The Jericho zircon chemistry is similar to compositions reported for mantle zircon megacrysts, but is distinct from fields previously reported for zircon occurring in glimmerite or MARID 1 xenoliths. (d) Model $^{207}Pb/^{206}Pb$ ages vs Th/U ratios for Jericho eclogite zircon. For some xenoliths such as JDLGS-011 MX1 (shaded field) there is a positive correlation, indicating the presence of multiple zircon components. Symbols are the same as in (c).

and 0·09–0·20, respectively) reported for kimberlite-borne eclogite xenolith CCS41 (Chen *et al.*, 1994). However, Jericho eclogite zircon compositions extend to slightly higher U and Th concentrations. The chemical composition of Jericho eclogite zircon are shown in Fig. 4c, together with the range obtained for mantle zircon megacrysts (Kresten *et al.*, 1975; Kinny *et al.*, 1989; L. M. Heaman, unpublished data, 2000), a high Th and U field for zircon isolated from Bultfontein MARID xenoliths (Kinny & Dawson, 1992), a second MARID field for zircon isolated from Kampfersdam xenoliths (Hamilton *et al.*, 1998), and a field for the range in zircon composition from glimmerite and harzburgite inclusions (Rudnick *et al.*, 1998). The Jericho eclogite zircon compositions overlap the low-U and low-Th field for mantle zircon megacrysts transported in kimberlites, and are distinct from other mantle-derived zircon, such as those

reported from glimmerite (Rudnick *et al.*, 1998) or MARID (Kinny & Dawson, 1992) xenoliths.

The Jericho eclogite zircons can be broadly subdivided into a lower-U suite with <35 ppm U (LGS046-MX8, LGS016-MX12 and LGS04-MX1) and a higher-U suite with U contents >45 ppm (LGS011-MX1 and LGS021-MX10). In addition, the higher-U suite exhibits a negative correlation between uranium content and Th/U ratio; this feature is not observed in the low-U suite. There is no correlation between uranium content or grain size vs model $^{207}Pb/^{206}Pb$ dates as xenoliths from both suites have zircon with a narrow range of uranium contents, but exhibit a large range in model $^{207}Pb/^{206}Pb$ dates. In most xenoliths there is a hint of a positive correlation between Th/U and model $^{207}Pb/^{206}Pb$ dates. This can be best seen in the data for four zircon analyses from xenolith LGS011-MX1 in Fig. 4d (shaded
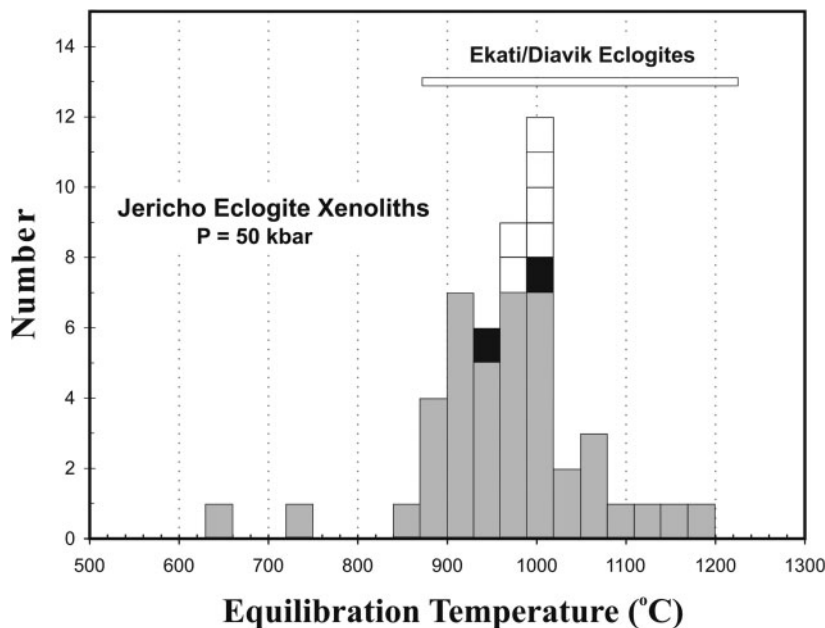
Fig. 5. Histogram of equilibration temperatures (calculated at a pressure of 50 kbar) for Jericho eclogites: white bars, diamond-bearing; black bars, zircon-bearing. Other eclogite types previously reported by Kopylova *et al.* (1999*a*, 2004) are represented by gray bars. For comparison the range of equilibration temperatures recorded in eclogites recovered from the Diavik and Ekati kimberlites in the central Slave craton are shown (Fung, 1998; Pearson *et al.*, 1999; Aulbach *et al.*, 2003).

region enclosing open diamonds). If there are multiple age components in these zircon grains (see below) then this correlation could reflect the fact that the younger zircon component has the highest U content and lowest Th/U.

GEOTHERMOMETRY

Garnet and clinopyroxene compositions were obtained for isolated crystals from two zircon-bearing eclogite xenoliths (MX8 and MX10) and several diamond-bearing eclogite xenoliths (Table 2). Compositional variation within and between grains is small and chemical zoning could not be discerned; thus we have confidence that the mineral chemical data obtained here can be used in a meaningful way to estimate relative equilibration temperatures for these xenoliths. Temperature estimates were calculated using the garnet–clinopyroxene Fe:Mg exchange thermometer of both Ellis & Green (1979) and Krogh-Ravna (2000) at a pressure of 50 kbar to facilitate direct comparison with temperature estimates reported from other studies (e.g. Kopylova *et al.*, 1999*a*, 2004; Pearson *et al.*, 1999). Equilibration temperatures calculated using the Ellis & Green (1979) thermometer are shown in Fig. 5 for the zircon-bearing (black bars) and diamond-bearing (white bars) eclogites from this study and a variety of Jericho eclogites reported previously by Kopylova *et al.* (1999*a*, 2004). Both the zircon- and diamond-bearing eclogites have equilibration

temperatures that overlap (948–1028°C) and are intermediate compared with the entire Jericho suite (850–1180°C; excluding two low-T xenoliths). The results presented here for the diamond-bearing eclogites are in agreement with the conclusion reached by Cookenboo *et al.* (1998*a*) that the diamond-bearing eclogites record very uniform equilibration temperatures of about 1000°C, with a total range of ∼30°C. The Jericho eclogite equilibration temperatures are similar to, but on average slightly cooler than, the range previously reported for eclogites recovered from other central Slave localities such as at Diavik (880–1210°C; Pearson *et al.*, 1999; Aulbach *et al.*, 2003) and at Ekati (725–1438°C; Fung, 1998).

ISOTOPE RESULTS
Analytical techniques

All isotope research was conducted at the University of Alberta Radiogenic Isotope Facility. Age calculations were performed using the program Isoplot (Ludwig, 1992) with the following decay constants: ^{87}Rb (1·42 × 10^{-11} year^{-1}), ^{147}Sm (6·54 × 10^{-12} year^{-1}), ^{238}U (1·55125 × 10^{-10} year^{-1}), and ^{235}U (9·8485 × 10^{-10} year^{-1}). The procedure for Rb–Sr phlogopite dating has been outlined by Creaser *et al.* (2004). Phlogopite macrocrysts and most minerals isolated from the eclogite xenoliths were liberated from uncrushed material with tweezers. Phlogopite analysed in this study was carefully

Table 5: Rb–Sr isotope data for phlogopite megacrysts from Jericho kimberlites JD-1 and JD-3, and entrained eclogite or peridotite xenoliths

Sample		Description	Weight(mg)	Rb(ppm)	Sr(ppm)	$^{87}Rb/^{86}Sr$	$^{87}Sr/^{86}Sr$
Kimberlite							
1	033710a	JD-1 megacryst	30·51	870	9·55	281·4	1·39638 ± 4
2	033710b	JD-1 megacryst	43·65	884	14·14	189·3	1·17357 ± 1
3	033710c	JD-1 megacryst	13·65	616	7·04	269·6	1·37114 ± 3
4	022888a	JD-1 megacryst	36·76	739	7·99	285·8	1·40517 ± 6
5	33711	JD-3 megacryst	43·42	443	2·67	543·6	2·05033 ± 3
Xenoliths							
6	JDLGS-017 MX14	JD-1 eclogite	27·52	390	24·63	46·35	0·81795 ± 4
7	JDLGS-011 MX1	JD-1 eclogite	27·27	115	15·56	21·40	0·75014 ± 5
8	JDLGS-011 MX1	JD-1 eclogite	9·68	234	39·02	17·20	0·76749 ± 3
9	JDLGS-011 MX1	JD-1 eclogite	6·10	305	179·59	4·840	0·71726 ± 1
10	33712	JD-3 peridotite	14·93	265	4·38	182·8	1·15600 ± 2

All phlogopite fractions were given a 2 h 0·7N HCl leach, except fraction 9, which was not leached. Uncertainties in $^{87}Sr/^{86}Sr$ ratios represent internal precision (95% confidence level). External reproducibility of $^{87}Rb/^{86}Sr$ ratios averages 1% (95% confidence level).

selected using a binocular microscope and generally represents the least altered material devoid of visible inclusions. The core regions of phlogopite megacrysts were isolated with a utility knife and then removed with tweezers to avoid margins of crystals that can be slightly chloritized. The uncertainties associated with the $^{87}Rb/^{86}Sr$ ratios listed in Table 5 average 1% (2σ) and the reported uncertainties in the $^{87}Sr/^{86}Sr$ ratios represent the measured 2σ internal precision obtained using a VG354 thermal ionization mass spectrometer operating in dynamic multi-collector Faraday mode. Total procedure blanks are <150 pg Sr and <200 pg Rb. During this study, an average $^{87}Sr/^{86}Sr$ value of 0·710269 ± 21 (1 SD; $n = 50$) was obtained for the NIST SRM987 strontium isotope standard and all unknowns were normalized to an accepted value of 0·710245.

The analytical procedure for purifying Sm and Nd from eclogite whole-rock, clinopyroxene and garnet and measuring their isotopic compositions using a VG354 thermal ionization mass spectrometer (dynamic multi-collector Faraday mode) generally follow the techniques described by Unterschutz *et al.* (2002). After the samples were weighed into pre-cleaned PFA Teflon digestion vessels, an aliquot of mixed ^{150}Nd and ^{149}Sm tracer solution was added and complete dissolution was accomplished using a combination of distilled 24N HF and 16N HNO_3 (5:1) and heating on a hotplate at 160°C for 4 days. The typical external reproducibility on an in-house Nd isotope standard is ±0·000016 (2σ). Total procedure blanks are <100 pg for both Sm and Nd. During this study the $^{143}Nd/^{144}Nd$ value obtained

for 34 analyses of the Shin Etsu Nd standard was 0·512097 ± 13 (1 SD).

Many of the mineral grains selected for U–Pb geochronology were extricated directly from uncrushed xenoliths. In some instances (e.g. xenolith MX8), a small portion of xenolith was lightly ground to a coarse aggregate to facilitate isolating individual crystals of apatite, garnet, rutile, and zircon. Minerals (except apatite) selected for U–Pb geochronology were washed in warm 4N nitric acid for 1 h, given a 1 min ultrasonic bath and then repeatedly rinsed in H_2O followed by acetone prior to weighing. All fractions were weighed with a Mettler UTM-2 ultra-microbalance, transferred to Teflon dissolution vessels with a measured amount of a ^{205}Pb–^{235}U tracer solution. Most minerals were dissolved using TFE Teflon vessels encapsulated in Monel jackets at a temperature of 220°C for ~120 h. Apatite was dissolved in 15 ml PFA Teflon capsules at 80°C using 6N HCl. The other minerals were dissolved using a 20:1 mixture of HF:8N HNO_3 for garnet, rutile and zircon, and a 1:1 mixture for perovskite. Following complete dissolution, the samples were evaporated to dryness and converted to chloride form by adding 0·5 ml of 3·1N HCl and heating overnight. Uranium and lead were purified using anion exchange chromatography following a procedure developed by Krogh (1973). Heat shrink Teflon exchange columns, of similar dimension to those described by Krogh loaded with DOWEX AG1 X8 200–400 mesh resin were used for all mineral fractions in this study. The purification procedure for zircon is similar to that described by Krogh (1973). The purification procedure
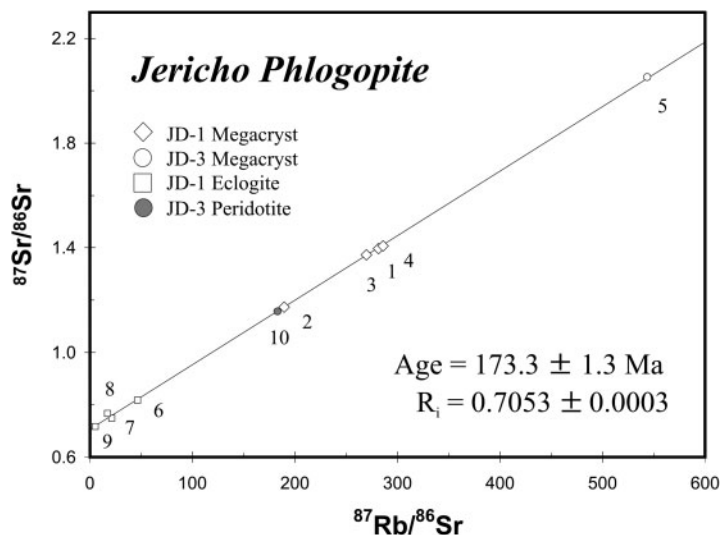
Fig. 6. Rb–Sr isochron diagram displaying isotopic data for phlogopite megacrysts isolated from JD-1 and JD-3 kimberlite, and from JD-1 eclogite and JD-3 peridotite xenoliths.

for all other minerals is similar to the 'HBr technique' described by Heaman & Machado (1992). Uranium and lead were eventually combined in the same pre-cleaned PMP beaker, a drop of 1·5N H_3PO_4 was added to facilitate location of sample, and the entire mixture was evaporated to dryness.

The isotopic compositions of uranium and lead were determined using a VG354 thermal ionization mass spectrometer operating in single collector mode. Both elements were loaded together onto outgassed high purity zone refined Re filaments using the Si gel technique of Cameron *et al.* (1969). The University of Alberta Si gel was prepared by distilling $SiCl_4$ into H_2O using PFA Teflon parts available from Savillex and constructed similar to more conventional two-bottle still designs. Loading blanks using this Si gel are <1 pg. This silica gel yields robust loads that provide stable Pb ion beams for several hours. The amount of Si gel used was empirically derived so that data collection for Pb was usually conducted in the temperature range 1450–1550°C. For most samples isobaric interference from organic molecules or thallium is negligible in this temperature range. Following data collection for Pb (minimum of 100 data collection cycles at three temperature increments), the filament temperature was raised to begin collection of uranium isotope data in the temperature range 1550–1650°C. Most of the isotopic data were obtained using a Daly photomultiplier detector (analog mode) and these data were corrected for detector bias (U: +0·15%/a.m.u.; Pb: +0·13%/a.m.u.) as well as for mass discrimination (U: +0·155%/a.m.u.; Pb: +0·088%/a.m.u.). Data reduction was accomplished with an in-house program and error evaluation for individual fractions calculated by numerically propagating 12 known sources of

uncertainty. The errors reported in Table 7 are quoted at 1σ absolute standard deviation. Age uncertainties are reported at 2σ.

Rb–Sr results for phlogopite megacrysts

The Rb–Sr results for ten phlogopite megacrysts hand-picked from kimberlite and mantle xenoliths are reported in Table 5. Two separate megacrysts were isolated from JD-1 kimberlite (033710 and 022888a) and one megacryst was analysed from JD-3 kimberlite (33711). The phlogopite megacrysts selected from the kimberlite samples consisted of fresh crystals generally devoid of visible inclusions or alteration. The majority of fractions (except fraction 9) were given a dilute (0·7N) warm HCl leach prior to dissolution, following the rationale of Brown *et al.* (1989). The unleached phlogopite contains an order of magnitude greater Sr content than the leached fractions, consistent with the observation of Brown *et al.* (1989) that many phlogopite megacrysts contain carbonate inclusions or carbonate residing along cleavage planes. The kimberlite-borne phlogopite megacrysts have higher Rb contents (443–870 ppm) and corresponding higher $^{87}Rb/^{86}Sr$ (189–543) compared with phlogopite isolated from xenoliths (115–390 ppm and 5–183, respectively). This demarcation is even more pronounced if only the $^{87}Rb/^{86}Sr$ of eclogite phlogopites (#6–9) are considered (5–46). The eclogitic phlogopite consistently contains higher Sr contents.

The Rb–Sr phlogopite results are displayed on an isochron diagram in Fig. 6. Considering only the phlogopite analyses from JD-1, which include three analyses from one megacryst (033710; #1–3) and one analysis from megacryst 022888 (#4), a best-fit regression line yields a age of 170·2 ± 4·3 Ma ($^{87}Sr/^{86}Sr_{initial} = R_i = 0·716 \pm$

Table 6: Sm–Nd isotope data for Jericho eclogite xenoliths

Xenolith no.		Mineral	Weight(mg)	Sm(ppm)	Nd(ppm)	$^{147}Sm/^{144}Nd$	$^{143}Nd/^{144}Nd$	ε_{Nd}(173 Ma)	T_{DM}(Ga)
1	JDLGS-017 MX14	Garnet	73·21	4·92	3·73	0·7978	0·513206 ± 7	−2·2	
2	JDLGS-017 MX14	Cpx	25·30	0·95	3·95	0·1458	0·512283 ± 10	−5·8	
3	JDLGS-011 MX1	WR	274·21	1·78	8·65	0·1248	0·512593 ± 9	0·7	0·98
4	JDLGS-046 MX8A	WR	251·16	9·81	53·1	0·1116	0·512328 ± 7	−4·2	1·25
5	JDLGS-046 MX8B	WR	237·53	9·14	51·3	0·1076	0·512356 ± 10	−3·5	1·16
6	JDLGS-046 MX8B	Garnet	229·13	4·32	3·80	0·6881	0·512956 ± 10	−4·7	
7	JDLGS-021 MX10A	WR	315·27	2·49	13·6	0·1105	0·512300 ± 9	−4·7	1·27
8	JDLGS-021 MX10B	WR	258·37	2·55	7·01	0·2202	0·512461 ± 9	−4·0	

Cpx, clinopyroxene; WR, whole-rock. Uncertainties in $^{143}Nd/^{144}Nd$ reported at 2σ. Uncertainty in $^{147}Sm/^{144}Nd$ estimated at <0·2% (2σ).

0·015; MSWD = 0·73). This age is interpreted to be a good estimate of the time of phlogopite formation and the time of JD-1 Phase 1 hypabyssal kimberlite emplacement. Including JD-3 megacryst 33711 ($t = 173·8 ± 5·2$ Ma; $R_i = 0·706 ± 0·008$; MSWD = 0·33) and JD-3 peridotite phlogopite #10 ($t = 173·2 ± 2·3$ Ma; $R_i = 0·706 ± 0·008$; MSWD = 1·19) does not change the age significantly. The model Sr date (assuming an initial $^{87}Sr/^{86}Sr$ value of 0·705) of 173 ± 2 Ma for JD-3 phlogopite megacryst 33711 is slightly older than the model ages for JD-1 phlogopite megacrysts, and partially explains why the composite phlogopite megacryst isochron date of 173·2 Ma is slightly older, with a lower initial strontium ratio than JD-1 megacryst results alone. A reference line constructed to pass through JD-3 phlogopite megacryst 33711 and phlogopite from a peridotite xenolith entrained in JD-3 yields a slightly older date of 173·7 ± 2·7 Ma with an unreasonably low initial strontium ratio of 0·70023. In summary, there is no discernible age difference between the Rb–Sr phlogopite ages for either JD-1 or JD-3, consistent with both pipes having a similar Jurassic emplacement age.

The eclogite Rb–Sr phlogopite results show more scatter. Fractions #7 and 8 clearly are not collinear with the other megacrysts, indicating that the Rb–Sr systematics in the eclogitic phlogopite could be more complex. A best-fit regression line using all data except phlogopite #7 and 8 yields a slightly more precise date of 173·3 ± 1·3 Ma ($R_i = 0·7053 ± 0·0003$; MSWD = 0·51). This date is considered the most reliable estimate for the emplacement ages of both the JD-1 and JD-3 kimberlites.

Sm–Nd results for eclogite whole-rock, garnet and clinopyroxene

The Sm–Nd isotopic composition for three eclogite whole-rocks (including two duplicates), two eclogitic garnets and one clinopyroxene are reported in Table 6

and displayed on an isochron diagram in Fig. 7. The Sm/Nd ratios for Jericho eclogite whole-rocks vary between 0·178 and 0·364 and overlap with those for oceanic basalts but trend toward slightly lower values than observed for them (0·26–0·36; Sun & McDonough, 1989). In contrast, the $^{143}Nd/^{144}Nd$ isotopic compositions for Jericho eclogite whole-rocks are variable (0·5123–0·5126), indicating that the eclogite xenoliths have variable ages, heterogeneous initial Nd isotope compositions, have been isotopically disturbed post formation (e.g. interaction with host kimberlite), or some combination of the above (whole-rock analyses are indicated by circles in Fig. 7).

A reference line with a slope corresponding to the 173 Ma kimberlite emplacement age based on the Rb–Sr phlogopite megacryst results is shown in Fig. 7, and there is clearly some disturbance in the Sm–Nd mineral systematics. For example, a reference line connecting garnet isolated from xenolith MX8B (#6) and whole-rock MX8B (#5) yields an age of 158 ± 8 Ma, slightly younger than the kimberlite emplacement age [similar 'young' internal isochrons have been reported for other eclogites; see, for example, Neal *et al.* (1990) and summary by Pearson (1999)]. On the other hand, an internal reference line constructed for garnet (#1) and clinopyroxene (#2) from eclogite MX14 yields an older internal age of 216 ± 8 Ma with an initial Nd isotope composition of 0·51208 ± 0·00003.

U–Pb results for kimberlite JD-3

Three small pieces of 2 inch kimberlite drill core were processed through crushing and mineral separation in an attempt to recover matrix perovskite. One sample of JD-1 (donated by M. Kopylova) contained minuscule individual matrix perovskite crystals (<15 μm in diameter) and thin perovskite rims on ilmenite, but perovskite was not successfully isolated from this sample.
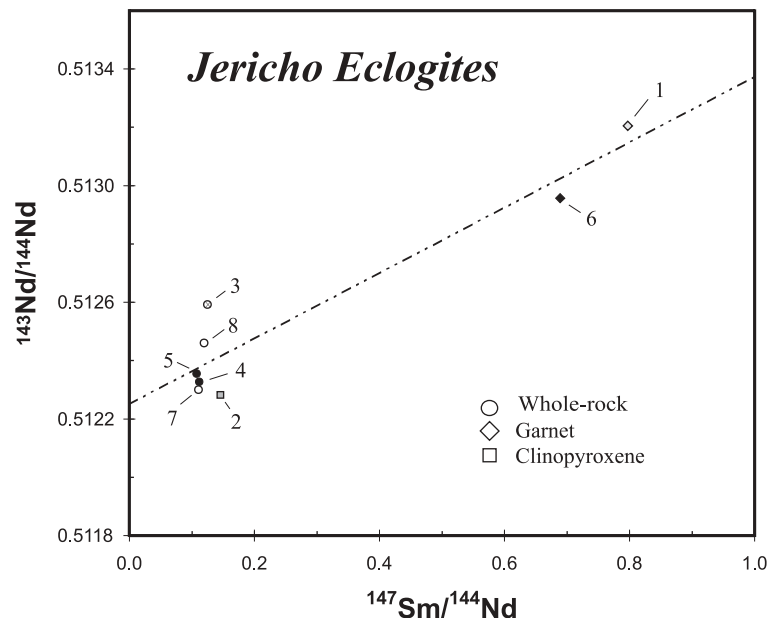
Fig. 7. Sm–Nd isochron diagram displaying isotopic data for eclogite garnet, clinopyroxene and eclogite whole-rocks (circles). ●, MX8; ○, MX10; circle with cross, MX11. The dashed line corresponds to a 173 Ma reference line.

Two small core samples from the same drill hole in JD-3 (donated by M. Kiridzija) contained larger (up to 70 μm) matrix perovskite and a few crystals were recovered. Perovskite in these two samples occurs as dark brown to black irregular fragments and parts of cubes.

The U–Pb results for three perovskite fractions, consisting of between six and 31 larger brown to black fragments or parts of cubes is presented in Table 7 and on a ^{238}U–^{206}Pb isochron diagram in Fig. 8. Perovskite in this sample contains moderate uranium (107–118 ppm) and has relatively high Th/U (72–80). The ^{206}Pb/^{238}U ages for these three perovskite fractions vary between 176·6 ± 3·2 Ma and 189·8 ± 3·4 Ma (2σ), which are generally older than the JD-3 Rb–Sr phlogopite megacryst (33711) model date of 173 ± 2 Ma reported above. The tendency for JD-3 perovskite to record U–Pb ages up to 17 Myr older than the JD-1 and JD-3 Rb–Sr phlogopite megacryst ages possibly indicates the existence of xenocrystic perovskite liberated from a kimberlite xenolith in this core sample from JD-3, a feature reported for a small number of kimberlites, such as the Elliott County kimberlite (Heaman *et al.*, 2004).

U–Pb results for eclogite apatite, garnet, rutile and zircon

Jericho eclogite xenolith MX8 contains the U-bearing minerals apatite, garnet, rutile and zircon. On the basis of the textural arguments presented above, garnet, clinopyroxene, zircon and possibly rutile are considered to have formed during eclogite metamorphism whereas apatite is probably a metasomatic mineral. The U–Pb

systematics of all four minerals (analyses #6–17 in Table 7) were investigated in an attempt to constrain the age of metamorphism and metasomatism. The closure temperatures to Pb diffusion in these minerals are different and probably vary from <400°C for apatite and rutile (e.g. Mezger *et al.*, 1989; Heaman & Parrish, 1991) to >900°C for zircon (e.g. Lee *et al.*, 1997). The closure temperature to Pb diffusion in garnet is poorly constrained. If the eclogite xenoliths remained at mantle temperatures >900°C, as indicated from geothermometry calculations (Kopylova *et al.*, 1999a, 2004; this study), until entrainment in Jericho kimberlite then we might anticipate that apatite and rutile (minerals with the lowest closure temperature) would have ages approaching those of kimberlite eruption. On the other hand, if the xenoliths had a more complex transport history (kimberlite magmatism in the Slave craton spans more than 600 Myr; Heaman *et al.*, 2003, 2004) then they may have resided at shallower mantle or crustal depths for much of their history and metamorphic or metasomatic age information might be preserved.

The U–Pb results for two apatite fractions (one of these was split after dissolution: 13A and 14A), one rutile (also split after dissolution) and one garnet fraction from eclogite MX8 are reported in Table 7 and shown on an isochron diagram in Fig. 8. The apatite analyses (#12–14) have relatively low uranium (10·9–11·2 ppm) and thorium (20·3–21·4 ppm) concentrations, which is most similar to Type B apatite (i.e. apatite in lherzolite xenoliths that have an origin linked to crystallization from an alkaline magma of kimberlite–carbonatite affinity)

Table 7: U–Pb isotope data for Jericho JD-3 kimberlite and JD-1 eclogite xenoliths

Weight (mg)	U (ppm)	Th (ppm)	Pb (ppm)	Th/U	TCPb (pg)	$^{206}Pb/^{204}Pb$	$^{238}U/^{204}Pb$	$^{206}Pb/^{238}U$	$^{207}Pb/^{235}U$	$^{207}Pb/^{206}Pb$	Model ages (Ma)			%Disc
											$^{206}Pb/^{238}U$	$^{207}Pb/^{235}U$	$^{207}Pb/^{206}Pb$	
JD-3 kimberlite														
1 P 0·206	106·9	8594	76·6	80·33	1810	39·695 ± 66	765·0 ± 2·4	0·0278 ± 5			176·6 ± 1·6			
2 P 0·100	117·7	8479·58	89·2	72·0	1033·86	39·845 ± 55	716·7 ± 1·8	0·0299 ± 3			189·8 ± 1·7			
3 P 0·058	113·75	8791·29	69·7	77·3	632	37·264 ± 105	655·4 ± 2·3	0·0287 ± 3			182·7 ± 1·8			
JDLGS-011-MX1														
2 Z 0·575	50·6	9·4	6·6	0·19	21	11241		0·1319 ± 3	1·500 ± 4	0·08248 ± 5	798·9 ± 1·9	930·6 ± 1·6	1256·9 ± 1·2	38·7
3 Z 0·331	62·3	5·7	2·7	0·09	29	1980		0·0436 ± 1	0·358 ± 1	0·05949 ± 9	275·2 ± 0·6	310·5 ± 0·7	585·3 ± 3·3	54·1
4 Z 0·154	50·6	11·0	4·3	0·22	8	4905		0·0814 ± 2	0·818 ± 2	0·07283 ± 10	504·7 ± 1·0	606·8 ± 1·2	1009·2 ± 2·9	52·0
5 Z 0·170	48·6	12·9	8·1	0·27	10	8873		0·1633 ± 4	2·131 ± 5	0·09464 ± 8	975·1 ± 2·0	1158·9 ± 1·6	1520·9 ± 1·6	38·6
JDLGS-046-MX8														
6 Z 0·226	11·4	1·4	0·7	0·12	27	347		0·0556 ± 3	0·493 ± 4	0·06434 ± 34	348·9 ± 1·8	407·2 ± 2·6	752·7 ± 11	55·1
7 Z 0·186	27·4	2·7	1·4	0·10	6	2865		0·0509 ± 1	0·463 ± 2	0·06589 ± 16	320·1 ± 0·7	386·0 ± 1·1	802·9 ± 5·1	61·6
8 Z 0·108	16·2	2·1	1·9	0·13	16	787		0·1111 ± 3	1·228 ± 6	0·08013 ± 31	679·4 ± 1·6	813·4 ± 2·7	1200·3 ± 7·6	45·7
9 Z 0·126	26·6	2·6	3·4	0·10	7	4058		0·1277 ± 3	1·628 ± 4	0·09251 ± 13	774·5 ± 1·5	981·2 ± 1·5	1477·8 ± 2·6	50·5
10 Z 0·225	11·7	1·1	1·9	0·10	25	1093		0·1618 ± 4	2·194 ± 6	0·09835 ± 16	966·8 ± 2·0	1179·2 ± 2·1	1593·1 ± 3·1	42·3
11 Z 0·231	22·5	1·5	1·0	0·07	26	533		0·0412 ± 1	0·341 ± 2	0·05996 ± 29	260·4 ± 0·5	297·8 ± 1·4	602·1 ± 10·6	57·9
12 A 3·853	11·1	21·4	14·5	1·94	>1000	18·760 ± 19	49·22 ± 12							
13 A 8·287	10·9	20·6	14·1	1·89	>1000	18·762 ± 19	49·98 ± 23							
14 A 8·287	11·1	20·3	13·6	1·83	>1000	18·773 ± 19	52·69 ± 27							
15 R 7·925	7·7	<0·1	0·3		879	137·27 ± 58	4359 ± 23	0·0273 ± 1	0·187 ± 3	0·04980 ± 70	173·4 ± 0·5	174·2 ± 2·3	185·5 ± 32·4	6·6
16 R 7·925	7·7	<0·1	0·3		914	132·41 ± 54	4210 ± 22	0·0271 ± 1	0·179 ± 3	0·04795 ± 73	172·2 ± 0·5	167·2 ± 2·4	96·6 ± 35·8	
17 G 7·771	0·031	<0·1	0·010		72	24·96 ± 45	236 ± 16	0·0276 ± 8			175·7 ± 5·1			
JDLGS-021-MX10														
18 Z 0·112	45·4	11·5	8·7	0·25	235	203		0·1375 ± 4	1·833 ± 11	0·09667 ± 51	830·6 ± 2·1	1057·3 ± 4·1	1560·8 ± 9·8	49·8
19 Z 0·129	52·5	11·7	11·0	0·22	626	93		0·1116 ± 3	1·438 ± 17	0·09348 ± 110	681·7 ± 1·9	904·8 ± 7·1	1497·7 ± 22	57·4
20 Z 0·178	52·6	6·9	2·5	0·13	174	121		0·0306 ± 1	0·232 ± 4	0·05478 ± 82	194·7 ± 0·6	211·5 ± 3·0	403·1 ± 33	52·5
21 Z 0·382	52·9	4·7	5·1	0·09	307	350		0·0808 ± 2	1·031 ± 4	0·09254 ± 28	500·8 ± 1·4	719·3 ± 2·3	1478·4 ± 5·7	68·7
JDLGS-016-MX12														
22 Z 0·160	33·4	7·3	1·8	0·22	27	633		0·0489 ± 1	0·407 ± 2	0·06030 ± 30	307·8 ± 0·7	346·4 ± 1·7	614·4 ± 11	51·1
23 Z 0·101	9·3	1·9	0·6	0·20	8	459		0·0633 ± 2	0·595 ± 9	0·06823 ± 93	395·4 ± 0·9	474·2 ± 5·4	875·7 ± 28	56·52
24 Z 0·208	17·6	5·7	3·8	0·32	259	141		0·1412 ± 5	1·693 ± 13	0·08694 ± 69	851·4 ± 2·5	1005·7 ± 5·1	1359·2 ± 15	39·9
25 Z 0·121	28·6	10·7	3·2	0·37	15·9	1331		0·0971 ± 2	0·973 ± 3	0·07271 ± 9	597·3 ± 1·3	690·2 ± 1·3	1005·9 ± 2·5	42·5
JDLGS-04-MX1														
26 Z 0·104	24·4	1·1	1·1	0·05	10	705		0·0451 ± 1	0·374 ± 3	0·06005 ± 51	284·5 ± 0·8	322·3 ± 2·5	605·3 ± 18	54·2

Mineral analysed: A, apatite; G, garnet; P, perovskite; R, rutile; Z, zircon. Th concentration is estimated from abundance of ^{208}Pb and corresponding $^{207}Pb/^{206}Pb$ ages. TCPb refers to the total amount of common Pb in picograms measured in the analysis. Atomic ratios are corrected for fractionation, blank, spike and common Pb (Stacey & Kramers, 1975). $^{206}Pb/^{204}Pb$ ratios are corrected for fractionation and spike only. All errors quoted in this table are 1σ uncertainties.
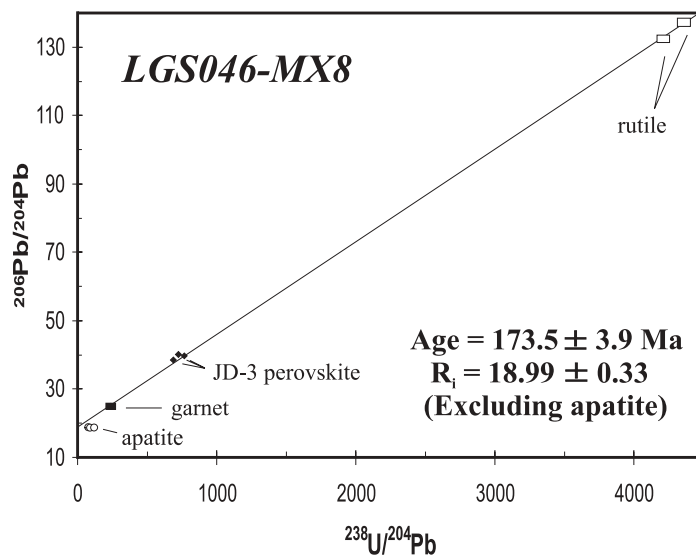
Fig. 8. U–Pb isochron diagram displaying isotopic data for JD-3 kimberlite matrix perovskite and for apatite, garnet and rutile isolated from eclogite xenolith LGS046-MX8.

described by O'Reilly & Griffin (2000). Of the minerals analysed from MX8 (excluding zircon below), apatite has the lowest $^{238}U/^{204}Pb$ (49–53) and $^{206}Pb/^{204}Pb$ (18·76–18·77). Both rutile and garnet have lower uranium concentrations (7·7 ppm and 31 ppb, respectively) than apatite but contain a higher percentage of radiogenic Pb with higher $^{238}U/^{204}Pb$ ratios of >4000 and 236, respectively. Interestingly, the Jericho rutile has an even higher proportion of radiogenic lead than JD-3 perovskite (see Table 7). Rutile from these zircon-bearing eclogites has relatively high uranium contents (7·7 ppm) compared with rutile from many other eclogites xenoliths, but overlaps within uncertainty the mean value of 3·9 ± 5·1 ppm (*n* = 22; e.g. Rudnick *et al.*, 2000; Barth *et al.*, 2001). The weighted average $^{206}Pb/^{238}U$ date of 172·8 ± 0·7 Ma for the eclogitic rutile duplicate analyses (173·4 ± 1·0 and 172·2 ± 1·0 Ma, respectively) and garnet (175·5 ± 10·2 Ma) is indistinguishable from the Rb–Sr phlogopite megacryst age of 173·1 ± 1·3 Ma.

The U–Pb results for MX8 apatite, garnet and rutile plus JD-3 perovskite are displayed on an isochron diagram in Fig. 8. The size of the symbols in Fig. 8 corresponds to the magnitude of the associated uncertainty for each analysis (except the symbols for perovskite, which are larger than the estimated error). The rutile, garnet and perovskite analyses all lie along a regression line, the slope of which corresponds to an age of 173·5 ± 3·9 Ma (MSWD = 80). This 173·5 Ma age is identical to the 173·3 ± 1·3 Ma composite Rb–Sr phlogopite age reported above and in general there is remarkable agreement among the different radiometric systems, all reflecting the time of Jericho kimberlite magmatism. The Jurassic U–Pb eclogite rutile and garnet dates reflect the

fact that both these minerals became closed systems to Pb diffusion at the time of kimberlite eruption. A relatively radiogenic initial $^{206}Pb/^{204}Pb$ ratio of 18·99 ± 0·33 is obtained if the apatite and two older perovskite (2,3) analyses are excluded from the regression calculation; this is interpreted to reflect the relatively radiogenic Pb isotopic characteristics of the Jericho kimberlite magma.

The U–Pb apatite results do not conform to this reference isochron and plot distinctly below it (Fig. 8) with $(^{206}Pb/^{204}Pb)_{173\ Ma}$ and $(^{207}Pb/^{204}Pb)_{173\ Ma}$ initial ratios that vary in the range of 17·34–17·42 and 15·39–15·41, respectively. These relatively unradiogenic Pb values are intriguing and probably reflect the fact that apatite formed from a different and lower $^{238}U/^{204}Pb$ reservoir than the other U-bearing minerals (e.g. during metasomatism).

Zircon was recovered from all 15 eclogite xenoliths listed in Table 1. Typically, the zircon crystals are up to 2 mm, colourless, subhedral, multi-faceted prismatic grains. The eclogitic zircon grains investigated so far generally have lower uranium abundances (9–62 ppm) and higher Th/U (0·05–0·37) compared with zircon from eclogite xenoliths within orthogneiss (100–300 ppm and <0·05, respectively; e.g. Peucat *et al.*, 1982; Creaser *et al.*, 1997, and references therein). The U–Pb results for 19 single zircon crystals extracted from five Jericho eclogite xenoliths are presented in Table 7 and displayed on concordia diagrams in Fig. 9a–d. Analysis numbers in Fig. 9 correspond to results presented in Table 7. At the scale of the plots, the individual error envelopes are difficult to see, so each analysis is represented by the calculated error ellipse surrounded by a circle. The U–Pb zircon results plotted
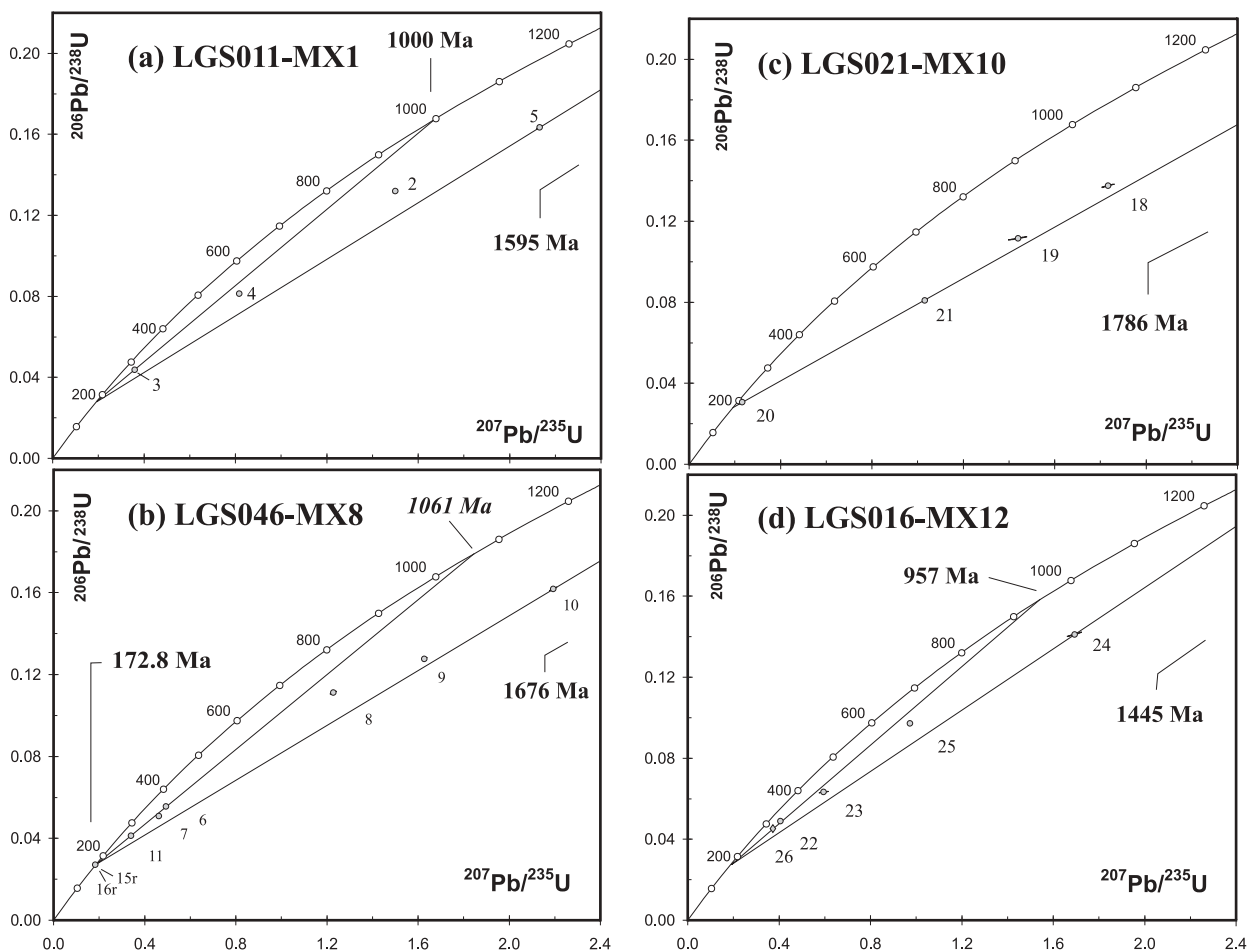
Fig. 9. U–Pb concordia diagrams for Jericho eclogite xenoliths. (a) LGS011-MX1; (b) LGS046-MX8; (c) LGS021-MX10; (d) LGS016-MX12.

for individual xenoliths in Fig. 9a–d display considerable scatter and, for the most part, do not define simple discordia or mixing lines. All the analyses are highly discordant (39–69%) and there is a large range in model $^{207}Pb/^{206}Pb$ dates for zircon suites from individual xenoliths.

The U–Pb results for four single zircon grain analyses from eclogite xenolith JDLGS-011-MX1 are displayed in Fig. 9a. The model $^{207}Pb/^{206}Pb$ dates vary between 585 and 1521 Ma and there is a correlation between model dates and Th/U. For example, the youngest zircon analysis #3 has the lowest model Th/U of 0·09. This relationship indicates multiple age and chemical components within individual zircon grains, with the youngest age component having low Th/U characteristic of 'metamorphic' zircon. The younger grains probably have a rim of very low Th/U component (perhaps also explaining the zoning visible in the CL image in Fig. 2c). Two reference lines are shown in Fig. 9a; both are anchored at the U–Pb rutile age of 172·8 Ma obtained from xenolith JDLGS-046-MX8 and constructed to pass

through the youngest and oldest grains, respectively. The upper intercepts of these lines indicate dates of approximately 1000 and 1595 Ma, respectively. The 1595 Ma date provides a minimum estimate for the age of the 'oldest' zircon component. The 1000 Ma date could reflect a Mesoproterozoic disturbance or growth of zircon in some grains.

The U–Pb results for six zircon (#6–11) and the duplicate rutile (15r, 16r) analyses from eclogite JDLGS-046-MX8 are displayed on a concordia diagram in Fig. 9b. The $^{207}Pb/^{206}Pb$ dates vary between 602 and 1593 Ma and the Th/U of these zircon grains is consistently low (0·07–0·13). Again, two reference lines are shown anchored at the weighted average $^{206}Pb/^{238}U$ rutile age of 172·8 Ma. Reference line 1 passes through analyses #6 and #11 and yields an upper intercept date of 1061 Ma. Reference line 2 was constructed to pass through the oldest zircon grain (#10) and yields and upper intercept date of 1676 Ma. These upper intercept dates are interpreted in the same manner as for xenolith JDLGS-011-MX1 above.

The most extreme range in $^{207}Pb/^{206}Pb$ dates was obtained for xenolith LGS021-MX10 (403–1561 Ma). Of the five eclogite xenoliths analysed, only the zircon grains isolated from this xenolith (Fig. 9c) closely approach a linear relationship where three of four analyses (#19–21) define a regression line with an upper intercept date of 1679 ± 10 Ma and a lower intercept date of 178 ± 5 Ma (37% probability of fit). Interestingly, this lower intercept date is within error of the kimberlite emplacement age of $173 \cdot 3 \pm 1 \cdot 3$ Ma established from Rb–Sr phlogopite megacrysts (see above). The reference line shown on the concordia diagram is constructed to pass through analyses 20 and 21, and yields an upper intercept date of 1786 Ma, interpreted as the minimum age of the 'oldest' zircon component. The zircon grains in this xenolith do not appear to be as strongly influenced by the Mesoproterozoic event as are those in other xenoliths.

The U–Pb results for zircon isolated from xenoliths JDLGS-016-MX12 (circles) and JDLGS-04-MX1 (diamond) are displayed in Fig. 9d. The four zircon analyses from JDLGS-016-MX12 have $^{207}Pb/^{206}Pb$ dates that vary between 614 and 1359 Ma with relatively high and consistent Th/U ($0 \cdot 20$–$0 \cdot 37$). As with xenolith JDLGS-011-MX1 above, the zircon grains with the higher Th/U have the older model dates. The two reference lines shown in Fig. 9d were constructed to pass through the oldest zircon grain (#24) and the youngest grains (#22 and 26), yielding upper intercept dates of 1445 Ma and 957 Ma, respectively. This discordance pattern is the same as seen in xenoliths JDLGS-011-MX1 and JDLGS-046-MX8; evidence for an old Paleoproterozoic zircon age component that has been modified or overgrown with a Mesoproterozoic episode of zircon growth. All zircon analyses have been moderately to strongly influenced by Pb loss or new zircon growth at the time of Jericho kimberlite magmatism and emplacement.

DISCUSSION
Nature and timing of Jericho kimberlite magmatism

The timing of Jericho kimberlite emplacement has been determined by four dating techniques and all four indicate a Jurassic emplacement age. The first approach investigated the Rb–Sr systematics of phlogopite megacrysts from two of the Jericho pipes (JD-1 and JD-3) and from entrained eclogite and peridotite xenoliths. Phlogopite in mantle xenoliths occurs as isolated grains, as replacement rims on garnet and clinopyroxene, and as an essential mineral component of veins. Although the origin of phlogopite in mantle xenoliths is controversial (Williams, 1932; Kushiro & Aoki, 1968; Carswell *et al.*, 1981; Hills & Haggerty, 1989; Taylor & Neal, 1989), the relatively low closure temperature to Rb and Sr diffusion

in mica ($\sim$500°C) implies that the Rb–Sr system in mantle phlogopite will record the time of kimberlite eruption. However, there could be a difference in the initial strontium isotopic compositions of phlogopite formed in different environments and this could lead to some scatter in the Rb–Sr isotope systematics. The majority of Jericho phlogopite megacrysts analysed in this study plot along a single isochron indicating a date of $173 \cdot 3 \pm 1 \cdot 3$ Ma (Fig. 6) and a relatively precise initial strontium ratio of $0 \cdot 7053 \pm 0 \cdot 0003$. These data indicate that there is no detectable difference in emplacement age between the Jericho JD-1 and JD-3 pipes. Furthermore, the reasonably good fit of most phlogopite analyses to the calculated regression line (MSWD = $0 \cdot 53$) indicates that the majority of phlogopite, including both xenolith and kimberlite megacrysts, must have formed from, or interacted with, the same homogeneous strontium reservoir.

The second approach used three groundmass perovskite fractions to obtain $^{206}Pb/^{238}U$ ages. The youngest of these three perovskite analyses yielded an age of $176 \cdot 6 \pm 3 \cdot 2$ Ma, which is within analytical uncertainty of the Rb–Sr phlogopite age of $173 \cdot 3 \pm 1 \cdot 3$ Ma. Although not a common occurrence, the older U–Pb perovskite ages could reflect the presence of a slightly older xenocrystic perovskite component in this sample, possibly derived from kimberlite xenoliths.

The third approach investigated the U–Pb systematics of eclogite minerals garnet and rutile. Rutile isolated from one eclogite xenolith entrained in JD-1 yields a weighted average $^{206}Pb/^{238}U$ date of $172 \cdot 8 \pm 0 \cdot 7$ Ma, in excellent agreement with the Rb–Sr phlogopite and youngest U–Pb matrix perovskite dates. Although the eclogite garnet analysis has a much lower $^{238}U/^{204}Pb$ (236) than the companion rutile (>4000), these two minerals plus the younger JD-3 matrix perovskite fraction define a precise isochron date of $172 \cdot 1 \pm 2 \cdot 1$ Ma, which is interpreted as a good independent estimate of the Jericho kimberlite emplacement age. The eclogite rutile and garnet formed in the mantle but record kimberlite emplacement ages because the eclogite xenoliths remained at mantle temperatures in excess of 900°C, which is greater than the closure temperature to Pb diffusion in both rutile ($\sim$400°C) and garnet ($\sim$700°C), until entrainment and probably rapid transport to the surface.

The fourth approach to estimating the time of Jericho kimberlite emplacement involved defining lower intercept ages by constructing reference lines to pass through discordant U–Pb zircon grain analyses from JD-1 eclogite xenoliths. The best-constrained U–Pb zircon lower intercept date of 178 ± 5 Ma is from xenolith MX10 (Fig. 9c).

All four approaches yield similar age results and indicate that a variety of radiometric dating techniques can be successfully applied to obtain geologically meaningful kimberlite emplacement ages. The more precise Rb–Sr phlogopite age of $173 \cdot 1 \pm 1 \cdot 3$ Ma is recommended as the

best estimate for the timing of kimberlite magmatism at Jericho. These age determinations corroborate the original findings of Heaman *et al.* (1997, 2002) and together document mid-Jurassic kimberlite magmatism in the northern Slave Province, Canada. Recently, Hetman *et al.* (2003) reported a similar Jurassic emplacement age (Rb–Sr; 173 ± 2 Ma) for the nearby Muskox kimberlite. The timing of Jericho–Muskox kimberlite magmatism is distinct from Jurassic kimberlite magmatism elsewhere in eastern North America, such as the 152–165 Ma Kirkland Lake field, 134–155 Ma Timiskaming field, or the 146–148 Ma Finger Lakes field (Heaman & Kjarsgaard, 2000), but these kimberlites do have a similar emplacement age to the oldest kimberlites (i.e. 176–180 Ma) in the Attawapiskat cluster in the James Bay lowlands (Heaman & Kjarsgaard, 2000).

The primary geochemical character of the Jericho kimberlites has been determined on chilled margin samples of aphanitic kimberlite dyke material by Price *et al.* (2000). These samples indicate that the Jericho primitive magmas had high MgO (20–25 wt %), high Mg-numbers (86–88), and high Cr (1300–1900 ppm) and Ni (800–1400 ppm) contents (Price *et al.*, 2000). The nature and origin of Jericho kimberlite magmatism can be further evaluated by investigating their radiogenic isotopic composition. Smith (1983) demonstrated that the majority of southern African kimberlites can be subdivided into two groups (Group I or Group II) based on their emplacement ages, mineralogical and isotopic character. The following isotopic ranges were reported for Group I and II southern African kimberlites, respectively: Group I have unradiogenic $^{87}Sr/^{86}Sr$ (0·7033–0·7049), relatively radiogenic $^{206}Pb/^{204}Pb$ (18·45–20·05) and positive ε_{Nd} (0·0 to +4·0) compared with Group II kimberlites (0·7074–0·7109, 17·2–17·7, and –5·0 to –8·0).

Dowall *et al.* (2003) reported radiogenic isotopic data for seven Jericho whole-rock kimberlite samples: $^{87}Sr/^{86}Sr$ between 0·7043 and 0·7084, and ε_{Nd} between +1·4 and +3·0. They concluded that the Jericho kimberlites are most similar to Group I kimberlites in southern Africa. The initial Sr isotopic composition derived from the Jericho phlogopite isochron (Fig. 6) of 0·7053 ± 0·0003 obtained in this study agrees with the range of whole-rock kimberlite compositions reported by Dowall *et al.* (2003) and just overlaps the highest values reported for southern African Group I kimberlites. The initial Pb isotopic composition of 18·99 ± 0·33 (Fig. 8) obtained in this study for eclogitic garnet and rutile may also reflect the composition of the host kimberlite magma. It is likely that these minerals may have involved some Pb isotopic exchange with kimberlite during magma transport, as they record the age of kimberlite magmatism and they have such low Pb contents (low ppm to ppb levels; Table 7) compared with primitive aphanitic Jericho kimberlite (13–24 ppm Pb; Price *et al.*, 2000). If this is the

case, then this radiogenic Pb isotopic composition also indicates an original magma composition most akin to Group I kimberlite. This pervasive Group I isotopic signature is interpreted to indicate that the Jericho kimberlite magmas are derived from a slightly depleted source region based on Nd isotopes (ε_{Nd} = +1·4 to +3·0; Dowall *et al.*, 2003) and a source region that also has a high-mu signature based on the radiogenic $^{206}Pb/^{204}Pb$ initial signature (this study).

Nature and timing of metasomatism

Kimberlite-borne eclogite xenoliths are typically modified geochemically by some form of metasomatism. In most cases the modification involves enrichment in Ba, Ca, K, light rare earth elements (LREE), Pb, Rb, and Sr with depletion of Na (e.g. Erlank *et al.*, 1987). The combination of elevated K and LREE in eclogite xenoliths, the presence of phlogopite rims on garnet, and alteration of metamorphic minerals can indicate chemical interaction between eclogite xenoliths and host kimberlite magma (e.g. Taylor & Neal, 1989) or upper mantle metasomatism (e.g. Hills & Haggerty, 1989).

Petrographic evidence indicates that there has been some interaction between kimberlite fluids or magmas and Jericho zircon-bearing eclogites. The most obvious features include the existence of patches and cross-cutting veins of alteration mineral assemblages including amphibole, barite, carbonate, phlogopite, and serpentine, ± chlorite (Fig. 2a). In addition, the serpentinization of clinopyroxene, which can be pervasive (Fig. 2b), and cross-cutting alteration micro-veinlets in apatite are probably formed by interaction with kimberlite magma. It is also possible that some eclogite phlogopite formed from interaction with kimberlite magma and after entrainment in Jericho kimberlite. This would explain the similar initial strontium isotopic composition for most eclogite phlogopite (0·7040–0·7054), the composite phlogopite isochron including five kimberlite phlogopite megacrysts (0·7053 ± 0003; Fig. 6) and the range reported previously for Jericho kimberlite whole-rocks (0·7043–0·7084; Dowall *et al.*, 2003). It also explains the similarity in mineral composition, in particular the low-BaO signature, between the eclogite phlogopite and the low-BaO cores of zoned phlogopite xenocrysts in Jericho kimberlite (e.g. Fig. 2f). It is also tempting to attribute most of the unusual whole-rock geochemistry (e.g. high MgO, very low SiO_2) of the Jericho eclogites to some form of contamination or interaction with Jericho kimberlite. Indeed, on many major element variation diagrams (e.g. Fig. 10) the measured Jericho eclogite whole-rock compositions plot between the composition of other kimberlite-borne eclogites [e.g. Koidu eclogites studied by Hills & Haggerty (1989)] and the host Jericho kimberlite.
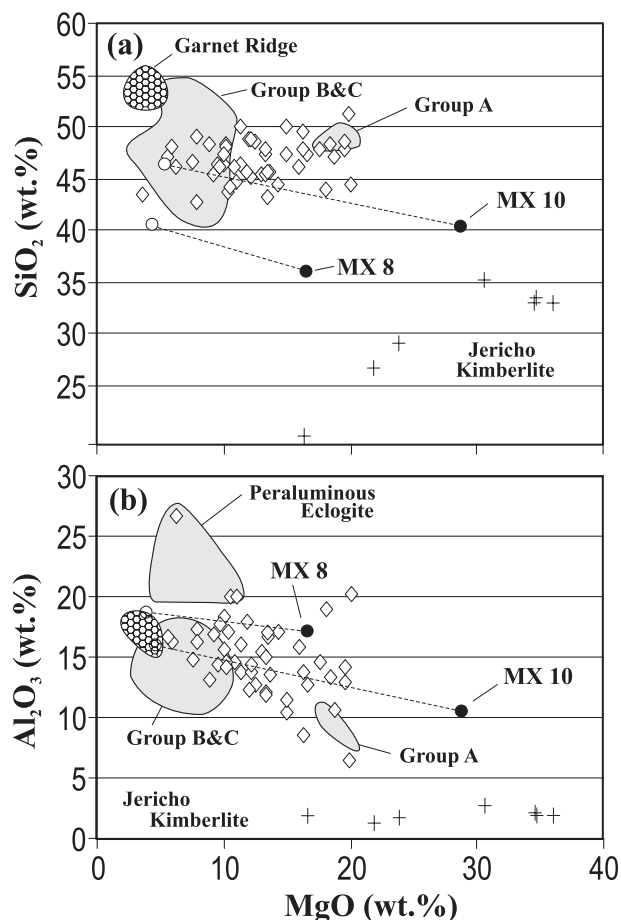
Fig. 10. Measured (●) and reconstructed (○) whole-rock compositions (connected by a dashed line) for two Jericho zircon/rutile-bearing eclogite xenoliths (MX8 and MX10). (a) SiO_2 vs MgO; (b) Al_2O_3 vs MgO. For comparison, fields for primitive, high-MgO Group A (e.g. eclogite xenoliths from Salt Lake crater, Hawaii; Green, 1966) and Group B and C eclogites (i.e. eclogite lenses within migmatite or orthogneiss and those exhumed at convergent margins, respectively) as summarized by Coleman *et al.* (1965) are indicated. In addition, previously published whole-rock chemical data for kimberlite-borne eclogite xenoliths (◇; primarily from Koidu, Roberts Victor and Bellsbank; Kushiro & Aoki, 1968; Shervais *et al.*, 1988; Hills & Haggerty, 1989; Taylor & Neal, 1989) are plotted. Also shown are fields for a peraluminous (>18 wt % Al_2O_3) eclogite suite that typically contains modal kyanite [(b) only; Hills & Haggerty, 1989] and a peculiar low-MgO/high-SiO_2 suite of eclogite xenoliths (hexagon pattern) from kimberlites in southwestern USA (Garnet Ridge, Arizona, and Moses Rock, Utah; Watson & Morton, 1969; Helmstaedt & Doig, 1975). +, Whole-rock chemical compositions reported for Jericho kimberlite JD-1, including chilled margin samples (Kopylova *et al.*, 1998*a*; Price *et al.*, 2000).

However, interaction between eclogite xenoliths and kimberlite magma cannot explain all the chemical or isotopic modification and alteration mineralogy observed in the Jericho eclogites. For example, such interaction does not account for the low measured content of relatively mobile elements, such as potassium and rubidium, in some eclogites. The eclogite whole-rock analyses

presented by Heaman *et al.* (2002) indicate low to moderate K_2O contents (0·03 and 0·64 wt %) compared with other kimberlite-borne eclogite xenoliths (mean = 0·55 ± 0·35; n = 44). In fact, eclogite MX8 has an unusually low K_2O content (0·03 wt %) compared with the host Jericho kimberlite (mean = 0·33 ± 0·17; n = 7; Kopylova *et al.*, 1998*a*; Price *et al.*, 2000), consistent with the absence of phlogopite in this xenolith. In this regard, eclogites MX8 and MX10 provide an interesting comparison because they have contrasting mineralogy; MX8 contains negligible phlogopite but is the only xenolith in this study that contains abundant apatite. This is clearly reflected in the whole-rock chemistry, as MX8 not only has low K_2O (0·03 wt %) but also low Rb (1·7–2·4 ppm) and transition metal contents, such as Ni (23 ppm) and Cr (14 ppm), and at the same time possesses much higher P_2O_5 (0·94 wt %), FeO (19·36 wt %), Sr (288–327 ppm) and REE contents (in particular LREE; Heaman *et al.*, 2002). The low alkali and transition metal contents in MX8 indicate that this xenolith was not significantly modified by interaction with Jericho kimberlite or a metasomatic fluid derived therefrom so any chemical modification [e.g. the high field strength element (HFSE) enrichment] must pre-date entrainment in the kimberlite magma. Zircon-bearing eclogite MX10, on the other hand, does have high K_2O (0·64%) and Rb (25 ppm), consistent with the presence of phlogopite, which could reflect interaction with kimberlite.

In addition to some geochemical inconsistencies, there is Nd isotope evidence that indicates that kimberlite contamination is not responsible for all the observed LREE enrichment in Jericho eclogites, even though Jericho kimberlite has high LREE contents (e.g. 72 ppm Nd; Price *et al.*, 2000). Most Jericho eclogite whole-rocks yield negative ε_{Nd} values (+0·7 to –5·8) calculated at 173 Ma, the time of kimberlite emplacement. If contamination by kimberlite were significant then one would anticipate a positive correlation between Nd content and isotopic composition of the eclogite. Seven samples of Jericho kimberlite have ε_{Nd} values between +1·4 and +3·0 (Dowall *et al.*, 2003) so the most contaminated eclogite should have the highest Nd content and the most positive ε_{Nd} composition. However, this is not the observed pattern, as eclogite MX1, with the highest ε_{Nd} of +0·7, actually has a relatively low Nd content of 8·65 ppm, and conversely eclogite MX8, with the highest Nd content of >50 ppm, has negative ε_{Nd} (–3·5 to –4·7). Therefore, it is unlikely that the scatter in ε_{Nd} values for Jericho eclogites is linked to host kimberlite contamination.

Considering the petrographic, geochemical and isotopic arguments presented above, we conclude that Jericho zircon-bearing eclogites preserve evidence for multiple periods of alteration–metasomatism. Apart from eclogite xenolith modification linked to interaction

with kimberlite magma discussed above, there is evidence for at least two other metasomatic overprints in some xenoliths (denoted as Type 1 and Type 2 in the following discussion).

Type 1 metasomatism

Type 1 metasomatism is responsible for the abundance and large size of refractory accessory minerals, such as zircon and rutile, and the HFSE-enriched nature of these xenoliths. As discussed by Heaman *et al.* (2002), the most spectacular geochemical aspect of the Jericho eclogite xenoliths is the magnitude of their HFSE enrichment: Nb 133–1134 ppm, Ta 5–28 ppm, Zr 1779–4934 ppm and Hf 23–64 ppm. The magnitude of this enrichment is profound when compared with the average composition for nearly 40 kimberlite-borne eclogite xenoliths: Nb $16\cdot2 \pm 12\cdot5$ ppm, Ta $0\cdot33 \pm 0\cdot22$ ppm, Zr $42\cdot9 \pm 17\cdot7$ ppm, and Hf $0\cdot73 \pm 0\cdot56$ ppm (Shervais *et al.*, 1988; Hills & Haggerty, 1989; Taylor & Neal, 1989; Rudnick *et al.*, 2000; Barth *et al.*, 2001). The Jericho eclogites not only have substantially elevated Nb contents compared with volcanic rocks from all oceanic settings and most other kimberlite-borne eclogite xenoliths, but also represent some of the most HFSE-enriched mantle-derived material. Residual rutile formed during high-degree partial melting of oceanic basaltic material would only enrich the Nb content of this residue by perhaps a factor of five at most (i.e. <10 ppm Nb), so a large proportion of the HFSE budget in these samples requires an external source (Heaman *et al.*, 2002).

Some of the Jericho eclogite xenoliths studied here are unique among kimberlite-borne eclogites in that they contain zircon. Zircon has a very high closure temperature to Pb diffusion (e.g. >900°C; Kinny & Dawson, 1992; Lee *et al.*, 1997; Cherniak & Watson, 2001), so the U–Pb zircon systematics could provide a more robust record of the pre-kimberlite history of these Jericho eclogite xenoliths. The large size of the zircon crystals, in particular, and their common association with garnet (i.e. they occur both as inclusions in garnet and also contain garnet inclusions) indicate that much of the zircon growth is intimately linked to garnet growth. The zircons that occur in alteration-rich domains tend to be anhedral and highly resorbed—further evidence that most zircon growth occurred prior to veining and the final period of metasomatism. The Jericho zircon is chemically distinct from metasomatic zircon formed in MARID xenoliths (e.g. Kinny & Dawson, 1992; Hamilton *et al.*, 1998), having much lower uranium contents and Th/U ratios (Fig. 4c), also consistent with a metamorphic origin.

The preservation of a multi-component age history in these eclogites is supported by both the complex internal structure preserved in the zircon crystals, with visible overgrowths that are especially revealed with CL imaging

(Fig. 2c), and the discordance pattern of the U–Pb data. The U–Pb zircon results for five Jericho eclogite xenoliths display a similar pattern with a large range of model $^{207}\text{Pb}/^{206}\text{Pb}$ dates between 403 and 1593 Ma with all analyses documenting moderate to high degrees of discordance (39–69%). These data either record a complicated multi-stage Pb-loss history or represent paleo-diffusion curves, such as those formulated by Nicolaysen (1957), Tilton (1960) and Wasserburg (1963) and evaluated by Peucat *et al.* (1982) for zircon from the Vendée eclogite and Baie d'Audierne garnet pyroxenite. Continuous diffusion of radiogenic Pb at high temperature results in zircon analyses that define curved trajectories on a concordia diagram. Such paleo-diffusion lines tend to approximate a linear relationship in the early part of the zircon history and display maximum curvature closer to the lower intercept date. Frozen paleo-diffusion curves could possibly account for the discordance patterns observed for xenoliths MX1 and MX8 (Fig. 9a and b, respectively) but would not fit the data from xenolith MX10 (Fig. 9c). Although continuous diffusion of Pb from zircon cannot be entirely ruled out for all xenoliths, we interpret the U–Pb data from MX10 as best reflecting a mechanism of episodic Pb loss or new zircon growth.

At least three dates can be gleaned from the U–Pb zircon data: Paleoproterozoic (>1·79 Ga) and Mesoproterozoic (0·96–1·06 Ga) upper intercept projections that are anchored by the time of kimberlite emplacement and the lower intercept date of 178 ± 5 Ma (Fig. 9). The difficulty is deciphering which date, if any, corresponds to the time of eclogite metamorphism, as this would place a minimum age constraint on the timing of Type 1 metasomatism. The Paleoproterozoic upper intercept dates can be explained in at least three ways: (1) the age of a primary mafic magmatic zircon component (minimum estimate given as 1786 Ma from xenolith MX10); (2) the age of an inherited Pb component from zircon xenocrysts; (3) the age of high-grade metamorphism ($\pm$ metasomatism).

Considering the possibility that the Paleoproterozoic zircon component is primary magmatic, it is important to note that very few mafic or ultramafic rocks (especially basalts) contain primary magmatic zircon (e.g. Black *et al.*, 1991). In mafic or ultramafic samples that do contain primary magmatic zircon the crystals tend to be small, often lacking well-developed crystal faces (forming shards), have moderate to high uranium contents (>200 ppm) and are characterized by rather high Th/U (>1; Bossart *et al.*, 1986; Heaman & LeCheminant, 1993), unlike the zircon recovered from Jericho eclogites (e.g. low U: <70 ppm; low Th/U: 0·05–0·37). A xenocrystic zircon origin for the Paleoproterozoic component is also possible, and is consistent with the correlation between high Th/U ratios and older $^{207}\text{Pb}/^{206}\text{Pb}$ dates recorded in some Jericho eclogite

zircons. However, zircon is a relatively rare mineral in mantle rocks, so it is difficult to envisage a process whereby zircon inheritance occurred in a mantle-derived mafic magma intruding the subcontinental lithosphere or from subducted oceanic lithosphere.

Petrographically, zircon occurs most commonly as subhedral inclusions randomly distributed in garnet and clinopyroxene (Fig. 2a). There is no evidence that the Jericho zircon is preferentially associated with alteration or veining. This, together with the low uranium contents and low Th/U, is taken as evidence for a dominantly metamorphic origin for the Jericho eclogite zircon. The oldest Paleoproterozoic zircon growth (>1786 Ma) probably occurred during initial eclogite metamorphism and the data scatter reflects subsequent thermal and/or metasomatic events that caused episodic Pb loss or new zircon growth. Our preferred interpretation is that Type 1 metasomatism occurred prior to, but associated with, Paleoproterozoic eclogite metamorphism. Further evidence for the Paleoproterozoic timing of HFSE enrichment, and hence Type 1 metasomatism, is the consistently old model Hf ages for Jericho zircon (2·1–2·3 Ga) and a similar old model Hf age for eclogite whole-rock MX8 (2·1 Ga) reported by Schmidberger *et al.* (2004).

Whether all the HFSE enrichment was extraneous, for example from interaction with fluids evolved from rutile-bearing carbonated eclogite perhaps in a subduction-zone environment (e.g. Dalton & Blundy, 2000), or the Jericho protoliths were unusually enriched in HFSE initially is unknown. There is some evidence that subducted oceanic crust can be enriched in HFSE during fluid–solid interaction (Sorensen & Grossman, 1989). Sorensen & Grossman demonstrated that garnet amphibolites that occur within the Catalina Schist, southern California have a mid-ocean ridge basalt (MORB)-like chemistry but have been enriched in Th, U, Sr, REE and HFSE during metasomatism involving fluids derived from subducted sediments. A similar process may have been involved in generating the ultra-enriched HFSE nature of the Jericho eclogite xenoliths prior to eclogite metamorphism. Regardless of the mechanism of HFSE enrichment, there is sufficient evidence to support the notion that many of the Jericho zircon-bearing eclogites examined in this study originally consisted of garnet–clinopyroxene–zircon–rutile ± ilmenite ± apatite and were enriched in HFSE prior to eclogite metamorphism and Type 2 metasomatism.

The timing of rutile formation is crucial to understanding the metamorphic history of these eclogites and the timing of Type 1 metasomatism, as Jericho rutile has a high Nb content and is the principal reservoir for Ti, Nb and Ta in the eclogite xenoliths. However, the U–Pb rutile date of 172·8 ± 0·7 Ma obtained for eclogite MX8 is identical to the Jericho kimberlite emplacement age determined by several methods and reflects the time at which rutile became closed to Pb diffusion at around 500°C (Mezger *et al.*, 1989; Cherniak, 2000). Therefore, the U–Pb rutile age indicates the time of kimberlite eruption when the eclogites were transported to the surface from ~150–180 km depth and not the time of metasomatism.

Type 2 metasomatism

Type 2 metasomatism is characterized by the growth of minerals such as apatite in MX8 and possibly carbonate, some high-TiO_2 phlogopite, and one or more Ba-rich minerals. The most noticeable geochemical fingerprint of Type 2 metasomatism is the high P_2O_5 (0·94 wt %) and Ba (>2000 ppm) contents, and LREE enrichment compared with other eclogite suites (e.g. Hills & Haggerty, 1989; Barth *et al.*, 2001). Type 2 metasomatism has some of the hallmarks of carbonatite metasomatism (e.g. Ionov *et al.*, 1993; Rudnick *et al.*, 1993; Yaxley *et al.*, 1998; O'Reilly & Griffin, 2000) including the growth of apatite, carbonate and phlogopite.

The origin of apatite in eclogite xenolith MX8 (possibly as much as 2·4 modal % based on the 0·94 wt % whole-rock P_2O_5 content in Table 8) is puzzling, as such apatite–zircon–rutile eclogite xenoliths are uncommon. At least one other apatite-bearing eclogite has been reported from Jericho (Kopylova *et al.*, 2004) and apatite-bearing eclogites have been reported from the Lac de Gras kimberlites (Jacob *et al.*, 2003). Apatite in MX8 may be part of the original protolith paragenesis, may have formed early in the history of this xenolith (associated with Type 1 metasomatism at ~1·8 Ga), during Type 2 metasomatism (see discussion below) or from interaction with Jericho kimberlite magma. The MX8 apatite has low U (11 ppm) and low Th/U (1·83–1·94), most consistent with Type B mantle apatite of O'Reilly & Griffin (2000), which those workers interpreted as reflecting an origin linked to carbonatitic fluids.

One of the unusual geochemical features of the Jericho zircon-bearing eclogites, and in particular the apatite–zircon–rutile eclogite MX8, is the extreme LREE enrichment. The average Nd content of bimineralic eclogites worldwide is 8 ± 3 ppm (e.g. Barth *et al.* 2001), so the Nd content of MX8 of >50 ppm represents a five-fold enrichment compared with most mantle eclogites. The majority of this Nd in MX8 (>40%) resides in apatite. It is, therefore, possible that the Nd isotope composition of these LREE-enriched eclogites could record the nature and timing of the metasomatic event responsible for this LREE enrichment and, possibly, the timing of apatite growth. In addition, the closure temperatures for Sm and Nd diffusion in garnet (Harrison & Wood, 1980; Coughlan, 1990; Van Orman *et al.*, 2002) are considerably higher (>800°C for a 1 cm garnet crystal) than many other mineral systems (e.g. Sr diffusion in micas <500°C;

Table 8: Measured and reconstructed whole-rock compositions for Jericho eclogites MX10 and MX8

Jericho MX10

								Reconstructed		Measured*
Present:	36·0	4·0	1·0	6·4	0·6	44·0	8·0		100·0	
Carb-free:	36·0	48·0	1·0	6·4	0·6			92·0		
	garnet	cpx	rutile	phlog	apatite	serp	carb	A	B	
SiO$_2$	37·62	56·24		39·79		48·00		46·83	39·46	40·39
Al$_2$O$_3$	21·57	13·12	0·72	14·79		2·00		16·32	10·12	10·37
TiO$_2$	0·10	0·14	90·90	4·48		0·02		1·41	1·24	1·24
FeO	26·54	6·97	2·50	7·95	0·40	0·60	0·22	14·61	10·65	10·62
MnO	0·76	0·04		0·04		0·04		0·32	0·29	0·24
CaO	9·02	9·72		0·01	51·00	0·05	38·97	8·93	7·08	7·08
MgO	4·10	5·64	0·01	18·21		49·00	48·00	5·81	28·27	28·80
K$_2$O				9·76				0·68	0·62	0·64
Na$_2$O	0·12	8·55		0·44				4·54	0·41	0·39
P$_2$O$_5$					37·40			0·24	0·22	0·22
	99·82	100·41	94·13	95·47	88·80	99·71	87·19	99·69	98·38	99·99

Jericho MX8

								Reconstructed		Measured
Present:	70·0	0·8	2·9	0·3	2·4	23·5	0·1		100·0	
Carb-free:	70·0	24·3	2·9	0·3	2·4			99·9		
	garnet	cpx	rutile	phlog	apatite	serp	carb	A	B	
SiO$_2$	37·79	56·41		39·79		40·00		40·32	36·42	35·83
Al$_2$O$_3$	21·77	14·33	0·94	14·79		2·00		18·81	15·90	17·11
TiO$_2$	0·07	0·13	91·42	4·48		0·02		2·75	2·72	2·76
FeO	26·26	6·61	1·65	7·95	0·40	0·60	0·22	20·09	18·66	19·36
MnO	0·66	0·03		0·04		0·04		0·47	0·47	0·44
CaO	8·66	8·57		0·01	51·00	0·05	31·97	9·38	7·40	6·74
MgO	4·73	4·98		18·21		53·00	25·00	4·58	15·88	16·67
K$_2$O				9·76				0·03	0·03	0·03
Na$_2$O	0·06	9·33		0·44				2·32	0·12	0·12
P$_2$O$_5$					37·40			0·90	0·90	0·94
	100·01	100·40	94·01	95·47	88·80	95·71	57·19	99·65	98·51	100·00

*Measured eclogite whole-rock composition from Heaman *et al*. (2002).
A, carbonate-free recalculated composition converting all serpentine into clinopyroxene. B, reconstructed composition using present-day estimate of modal mineralogy.

Hart, 1964); thus there is some potential that geologically meaningful pre-kimberlite Sm–Nd formation, or metamorphic or metasomatic ages, could be preserved in these eclogites.

Most previous whole-rock eclogite Nd isotope studies indicate significant modification from interaction with host kimberlite (e.g. Jagoutz, 1988); thus, reconstructed bulk-rock isotopic compositions are considered the most robust indicator of the primary eclogite signature (e.g. Jacob *et al.*, 2005). Unfortunately, reconstructed bulk-rock Nd isotopic compositions are not possible with the current Jericho eclogite data. However, it is considered

significant that the model Nd T_{DM} ages for the zircon-bearing eclogites are relatively consistent and vary between 0·98 and 1·27 Ga (Table 6). These Mesoproterozoic model ages can be interpreted to indicate that the Jericho eclogites were either derived from protoliths of about this age or, considering the Paleoproterozoic U–Pb zircon ages discussed above, more probably indicate that there was a significant LREE enrichment or equilibration event (e.g. metamorphism, metasomatism, or thermally driven equilibration) that took place at about this time. We, therefore, interpret these Mesoproterozoic model Nd dates to record the time of Type 2 metasomatism. Similar Mesoproterozoic reconstructed model Nd ages were reported for eclogites from the Ekati kimberlites (Jacob *et al.*, 2003), ~150 km to the south, indicating that this Type 2 metasomatic event is recorded over a relatively large region of the Slave mantle lithosphere.

Additional support for a Mesoproterozoic metasomatic and/or thermal event is recorded in the secondary U–Pb zircon upper intercept ages. The upper intercept dates for the youngest zircon grains are relatively consistent and vary between 957 and 1061 Ma, overlapping the younger model Nd eclogite whole-rock dates (Table 6) and one of the peaks of Re depletion ages recorded in Jericho peridotite xenoliths (Irvine *et al.*, 1999, 2001). It is unclear at this point whether the range between 0·96 and 1·27 Ga in young zircon upper intercept and model Nd dates reflects the influence of more than one Proterozoic thermal and/or metasomatic event in the Slave subcontinental mantle or not. We note that the older model dates are close in time to the 1·27 Ga Mackenzie Igneous Event (LeCheminant & Heaman, 1989). Interestingly, Jericho peridotite xenoliths record model Re depletion dates that vary between 3·1 and 0·5 Ga (Irvine *et al.*, 2001), with a peak of model dates in the 1·2–1·5 Ga range, similar to many of the model Nd dates reported here. Irvine *et al.* interpret this young peak in model dates to reflect Re–Os modification by large-scale thermal or magmatic events such as the 1·27 Ga Mackenzie Igneous Event (LeCheminant & Heaman, 1989). Significant Slave lithosphere modification during the Mackenzie Igneous Event is further supported by the occurrence of 1·28 Ga metamorphic or metasomatic zircon growth in lower crustal mafic granulite xenoliths (Davis, 1997). If the Mesoproterozoic model Nd ages and the secondary U–Pb zircon upper intercept ages reflect the approximate time of Type 2 metasomatism, then it is younger than all known Precambrian alkaline magmatism in the Slave craton (e.g. the youngest being the 2023 +4/–2 Ma Booth River Intrusive Suite; Cavell & Baadsgaard, 1986; Villeneuve & Relf, 1998). Other known large mafic magmatic events that may have influenced the Slave mantle lithosphere are the 0·78 Ga Gunbarrel Igneous Event (LeCheminant & Heaman,

1994; Harlan *et al.*, 2003) or the 0·72 Ga Franklin Igneous Event (Heaman *et al.*, 1992).

The isotopic composition of the Type 2 metasomatic fluid may be preserved by the Pb isotope composition of eclogitic apatite. The U–Pb eclogite apatite data plot below the reference isochron constructed in Fig. 8, defined by garnet, rutile and perovskite, and apatite is clearly not in isotopic equilibrium with these minerals. In fact, the majority (~50%) of the Pb in the MX8 whole-rock (0·84–1·20 ppm; Heaman *et al.*, 2002) is hosted in apatite. The apatite initial lead isotope compositions calculated using a 173 Ma age yield $^{206}Pb/^{204}Pb$ and $^{207}Pb/^{204}Pb$ values of 17·32–17·41 and 15·39–15·41, respectively; these are significantly less radiogenic than the isochron initial $^{206}Pb/^{204}Pb$ value of 18·99 ± 0·33, which is controlled largely by the garnet and rutile analyses. These initial Pb isotope compositions for apatite are interpreted to reflect the relatively unradiogenic Pb isotopic characteristics of the Type 2 metasomatic fluid.

Finally, the occurrence of an armalcolite inclusion in rutile from MX8 provides additional evidence for a metasomatic event. Armalcolite is known to occur in kimberlite-borne xenoliths (e.g. Haggerty, 1983, 1994) and, in most cases, armalcolite is considered to form as a metasomatic mineral in upper mantle xenoliths. The armalcolite inclusion in rutile in MX8 could have formed during a stage of metasomatism that occurred prior to rutile growth (i.e. during Type 1 metasomatism), but we cannot rule out the possibility that armalcolite formation occurred after rutile growth through fluid infiltration along fractures (e.g. during Type 2 metasomatism or kimberlite interaction).

Primary nature of Jericho eclogites?

Elucidating the original mineralogy and primary composition of the Jericho eclogite protoliths is challenging, as their complex history, involving metamorphism and multiple episodes of metasomatism, has combined to produce a rock that, in some instances, is unlike its protolith. One of the primary goals of attempting to ascertain the nature of their protoliths is to determine whether they may have an origin linked to high-pressure mafic or ultramafic magmas that crystallized at great depth (>150 km) in the mantle (an origin that has been proposed for Jericho diamond-bearing eclogites; Cookenboo *et al.*, 1998*c*), or whether they could represent pieces of subducted oceanic crust and would, therefore, have a chemical composition similar to some type of oceanic basalt (an origin that has been proposed for other Jericho bimineralic eclogites; Kopylova *et al.*, 1999*a*).

Mantle eclogite xenoliths can be subdivided based on a mineral chemistry classification scheme proposed by Coleman *et al.* (1965): Group A eclogites contain garnet

and clinopyroxene with very high MgO contents (>13 wt %), consistent with an ultramafic protolith such as a picrite or a cumulate from a mantle-derived basaltic or komatiitic melt, Group B eclogites have an intermediate mineral chemistry, and Group C eclogites contain low MgO–high-FeO garnets and high-Na_2O clinopyroxene, most similar to eclogite mineral compositions that occur in convergent margin environments, or those associated with glaucophane schists (these divisions are outlined in Fig. 3). Group C mantle eclogite xenoliths are common in ultramafic diatremes located in the Four Corners region, USA (e.g. Garnet Ridge, Moses Rock, Mule Ear diatremes); here several researchers have noted similarities to Franciscan eclogites and have proposed a link to subducted oceanic lithosphere (e.g. Helmstaedt & Doig, 1975; Helmstaedt & Schulze, 1989).

The Jericho eclogitic garnet and clinopyroxene compositions determined in this study and by Kopylova *et al.* (1999*a*, 2004) have been compared with a worldwide database for eclogite xenoliths at well-known localities in Africa, Russia and the USA (e.g. Watson & Morton, 1969; MacGregor & Manton, 1986; Shervais *et al.*, 1988; Hills & Haggerty, 1989; Taylor & Neal, 1989; Jerde *et al.*, 1993; Beard *et al.*, 1996; Snyder *et al.*, 1997; see also compilation by Jacob, 2004). Clinopyroxenes from the majority of mantle eclogites have intermediate compositions and plot within the Group B field of Coleman *et al.* (1965). This includes clinopyroxenes from most of the known diamond-bearing eclogites, such as the Koidu diamond-bearing eclogite field shown in Fig. 3b. According to this mineral chemistry classification scheme, the Jericho zircon-bearing eclogites are exclusively Group C and the diamond-bearing eclogites are exclusively Group A, indicating that these two eclogite suites represent completely different protoliths.

Jericho diamond-bearing eclogites

The Jericho diamond-bearing eclogites have a much more simple mineralogy than the zircon-bearing eclogites and they tend to be less altered. The remarkable feature of the Jericho diamond-bearing eclogites is their uniform mineral chemistry with high-MgO garnet (19·6–21·3 wt %) and clinopyroxene (16·6–17·0 wt %), probably reflecting an ultramafic protolith. Compared with garnet from other eclogite suites, Jericho diamond-bearing eclogitic garnet is identical to high-MgO eclogitic garnets reported from some xenoliths recovered at Koidu (Hills & Haggerty, 1989), nine eclogite xenoliths from Roberts Victor (MacGregor & Manton, 1986), and two eclogite xenoliths from Bellsbank (Shervais *et al.*, 1988). Interestingly, the garnet compositions for Jericho diamond-bearing eclogites are much more magnesian than diamond-bearing eclogites from most other occurrences in Africa or Russia (see compilation by Jacob, 2004).

Similarly, clinopyroxene from diamond-bearing eclogite at Jericho has a remarkably uniform composition that is very different from the majority of diamond-bearing eclogites elsewhere, with a distinctive high-MgO–low-Na_2O signature (Fig. 3b), plotting within the field for a small number of ultrahigh-MgO eclogites from Koidu (Hills & Haggerty, 1989), Roberts Victor (MacGregor & Manton, 1986), and Udachnaya (Snyder *et al.*, 1997). In general, the high-MgO ultramafic protolith for the Jericho diamond-bearing eclogites is not a common source rock for diamond growth. This is substantiated by the observation that eclogitic clinopyroxene inclusions in diamond (not shown), such as those in Kankan diamonds (Stachel *et al.*, 2000), have compositions within the field for Group B eclogite, where most diamond-bearing eclogite xenoliths plot.

Jericho zircon-bearing eclogites

The primary nature of the Jericho zircon-bearing eclogites is much more difficult to unravel because they have been modified by at least two periods of metasomatism. However, there are four main pieces of evidence that hint at the original nature of their protolith(s): (1) mineral chemistry; (2) reconstructed whole-rock compositions; (3) stable mineral inclusions; (4) Nd isotope compositions.

Mineral compositions

The principal mineralogy in the Jericho zircon-bearing eclogites is characterized by high-FeO (23–28 wt %) garnets and highly jadeiitic clinopyroxene (i.e. 8·5–9·4 wt % Na_2O). In fact, garnets from the Jericho zircon-bearing eclogites have the lowest MgO contents and highest FeO contents of any kimberlite-borne eclogite, except for an unusual suite of high-FeO eclogitic garnets from xenoliths entrained in ultramafic diatremes located in the Four Corners region, USA (Watson & Morton, 1969; McGetchin & Silver, 1970; Helmstaedt & Doig, 1975; Helmstaedt & Schulze, 1989). Another interesting geochemical feature of these eclogites is the high Al_2O_3 content in the clinopyroxene (13·12–14·33 wt %). Taken together, the garnet and clinopyroxene compositions hint at protoliths that have elevated FeO, Na_2O and Al_2O_3 contents.

The high-Al_2O_3 (0·57–0·99 wt %) nature of the zircon-bearing eclogite rutile provides additional chemical evidence for a high-Al_2O_3 basaltic protolith. Rutiles that occur in kimberlite-borne eclogite xenoliths (open squares and triangles in Fig. 4a) have very low Cr_2O_3 contents ($<0·25$ wt %) and a large range in Al_2O_3 contents. Rutile crystals from kyanite eclogite xenoliths (open triangles) contain the highest Al_2O_3 compositions (0·51–1·21 wt %), indicating that rutile compositions might serve as a useful proxy for the nature and composition of the protolith. The Jericho rutile compositions are

also enriched in Al_2O_3 compared with rutile from most other kimberlite-borne bimineralic eclogites (Fig. 4a and b) and fall within the range for rutile from peraluminous eclogite. This high-alumina character probably indicates the breakdown of a high-aluminum mineral, such as feldspar or aluminous pyroxene, during its formation. In some respects the Jericho rutiles have a typical eclogitic low-Cr_2O_3 composition, which is consistent with derivation from a mafic protolith (compared with the high-Cr rutiles in ultramafic xenoliths, Fig. 4a). However, Jericho MX8 rutile is compositionally distinct, having both high Al_2O_3 and high Nb_2O_5 (Figure 4b). This high-Nb_2O_5 character is probably a signature acquired from carbonatite metasomatism that pre-dates rutile formation and is probably responsible for early armalcolite genesis. Although Jericho rutile contains moderately high Nb contents compared with many other eclogitic rutile (e.g. Hills & Haggerty, 1989), some rutiles in LIMA inclusions, such as those entrained in Jagersfontein or Orapa kimberlite (Haggerty, 1983), can have much higher Nb_2O_5 contents (up to 21 wt % in the Nb–Cr rutiles from Orapa; Tollo & Haggerty, 1987).

Reconstructed whole-rock compositions

Whole-rock compositions of kimberlite-borne mantle xenoliths can be significantly modified by interaction with metasomatic fluids or the host kimberlite magma prior to or during transport from the mantle; consequently, many researchers prefer to evaluate the primary chemical composition of eclogites by reconstructing their composition based on primary mineral chemistry and modal compositions (e.g. Rudnick *et al.*, 2000; Barth *et al.*, 2001, 2002; Jacob, 2004). However, it is not straightforward directly to determine the exact primary modal composition of the Jericho zircon-bearing eclogite xenoliths because they are rather coarse grained, they contain significant amounts of alteration, they have an unusual accessory mineral suite, and the amount of material available to study is small. In cases where relatively accurate modal compositions have been determined (e.g. Hills & Haggerty, 1989), the range in modal garnet and pyroxene in bimineralic eclogite typically varies between ~35 and 60 modal %.

The reconstructed whole-rock compositions for two Jericho zircon-bearing eclogite xenoliths are presented in Table 8. The most significant alteration component in these xenoliths is serpentine (up to 90% of the clinopyroxene has been altered to serpentine in some xenoliths) and carbonate. It is possible to derive an approximate present-day modal mineralogy for the two eclogite xenoliths by attempting to match the measured whole-rock composition by varying the modal proportion of the minerals in the following order: garnet (MnO, Al_2O_3 and FeO), clinopyroxene (Na_2O), phlogopite

(K_2O), apatite (P_2O_5), and rutile (TiO_2). The remaining elemental deficiencies can be approximated by using average mineral compositions for serpentine and carbonate (as given in Table 8). The best geochemical matches (compare column B with the measured whole-rock compositions in Table 8) are achieved when the following present-day modes are assumed: MX10—36·0% garnet, 4·0% clinopyroxene, 1·0% rutile, 6·4% phlogopite, 0·6% apatite, 44·0% serpentine, 8·0% carbonate; MX8—70% garnet, 0·8% clinopyroxene, 2·9% rutile, 0·3% phlogopite, 2·4% apatite, 23·5% serpentine, 0·1% carbonate. To achieve the modal estimates, a range of serpentine compositions was used in Table 8. If this approach provides an approximate estimate of the present-day modes, then the original modal mineralogy for these two xenoliths must have been variable. If we assume that all the serpentine was derived by alteration of original clinopyroxene, then we can estimate the original modal abundances of garnet and clinopyroxene and arrive at a pre-alteration whole-rock composition (column A). The resulting pre-alteration modes indicate that MX10 contained 36% garnet and 48% clinopyroxene whereas MX8 contained 70% garnet and 24% clinopyroxene.

There are two reconstructed whole-rock compositions listed in Table 8; composition A is the best estimate for the original eclogite whole-rock composition prior to the latest alteration (i.e. prior to any serpentinization and carbonatization), and composition B is based on considering the current mineralogy including the alteration mineral assemblage. The estimated pre-alteration reconstructed whole-rock compositions (column A) indicate that both xenoliths must have had a high-FeO (14·6, 20·1 wt %), high-Al_2O_3 (16·32, 18·81 wt %), high-TiO_2 (1·41, 2·75 wt %) and ultralow-MgO (4·58, 5·81 wt %) basaltic parentage (SiO_2 varies between 40·3 and 46·8 wt %), not unlike a variety of oceanic and continental basaltic rocks (e.g. Macdonald & Katsura, 1964; Pearce *et al.*, 1995). The ultralow-MgO reconstructed bulk-rock compositions for these Jericho zircon-bearing eclogites are even lower than other 'low-MgO' eclogite xenoliths, such as the low-MgO and kyanite-bearing eclogites from Koidu (6·2–10·1 wt %; Hills & Haggerty, 1989). The relatively high sodium contents (reconstructed Na_2O varies between 2·3 and 4·5 wt %) could reflect the possibility that the basaltic precursors experienced spilitization and/or contained significant plagioclase. It is clear that the present-day high whole-rock MgO and low SiO_2 contents reflect significant serpentinization, probably in large part from interaction with the host Jericho kimberlite magma. The measured whole-rock eclogite compositions (filled circles) clearly trend towards the Jericho kimberlite field in Fig. 10 and support the notion of some modification by, or interaction with, Jericho kimberlite.

Another piece of whole-rock geochemical information that could provide a clue to the protolith for some Jericho eclogites is the slight positive Eu anomaly preserved in the three zircon-bearing eclogites reported by Heaman *et al.* (2002) and two eclogites reported by Kopylova *et al.* (2001). Although the LREE have been modified by metasomatism, it is possible that this positive Eu anomaly records the prior existence of a mineral that concentrates Eu^{2+}, such as plagioclase. The relatively high bulk-rock Al_2O_3 composition obtained for xenolith MX8 (17·11 wt %; Heaman *et al.*, 2002) and even higher recalculated composition of 18·81 wt % (Table 8) could also indicate the original accumulation of an aluminous mineral such as feldspar in this xenolith.

Mineral inclusions

Another clue to the possible original protolith mineralogy of these eclogites is the nature of their mineral inclusions. Ilmenite forms an inclusion phase in both zircon and rutile in the Jericho zircon-bearing eclogites. This provides some evidence that ilmenite may have been a primary mineral in the protolith of several Jericho eclogites—a conclusion also reached by Meyer & Boctor (1975) for Stockdale eclogites. Ilmenite has been reported in many Jericho eclogites, including some studied by Kopylova *et al.* (2004).

Isotopic evidence

In addition to mineral chemistry, the primary Sr, Nd and Pb isotope signature of the eclogite xenoliths could reveal important information concerning their origin. Although most of the isotopic systems studied in the Jericho eclogites have been disturbed by metasomatism and/or interaction with kimberlite, it is possible that some primary isotopic signatures for the most robust systems are still preserved. The initial Sr isotope composition of 0·7053 from the phlogopite isochron in Fig. 6 is interpreted to reflect the isotopic composition of the host Jericho kimberlite and so does not reflect the primary eclogite composition. Similarly, the initial Pb isotope data from eclogite garnet and rutile are interpreted to reflect the isotopic nature of the host kimberlite, not the eclogite protolith. On the other hand, the eclogite whole-rock Nd isotope compositions do preserve some hint of the protolith composition, despite variable LREE enrichment during Type 2 metasomatism. Eclogite xenolith MX1 is the only zircon-bearing eclogite in this study that yields a positive ε_{Nd} value of +0·7 (calculated at the time of kimberlite emplacement) together with a low Sm/Nd of 0·21, which is only slightly lower than average basalt. In fact, the eclogite ε_{Nd} values become increasingly more negative with lower Sm/Nd (i.e. higher Nd contents), consistent with a metasomatic overprint; thus, we interpret the ε_{Nd} value of +0·7 as a minimum estimate

of the original protolith signature. A primary eclogite Nd isotope signature more positive than +0·7 indicates that the protolith(s) was probably derived from a depleted mantle reservoir, such as a piece of subducted oceanic crust. Such a signature would also be consistent with a primitive mantle-derived mafic magma with a chondritic ε_{Nd} signature of zero that was contaminated to some degree with a depleted mantle component prior to metasomatism. Our preferred interpretation is that the protoliths to these Jericho zircon-bearing eclogites initially had a depleted mantle Nd signature (i.e. positive ε_{Nd}), similar to mid-ocean ridge and some ocean island basalts, and that this signature was overprinted by an ancient (i.e. Precambrian) metasomatic event that featured an LREE-enriched fluid characterized by negative ε_{Nd} and low Sm/Nd. This interpretation is supported by the fact that the eclogite xenoliths with the highest Nd concentrations (e.g. MX8 in Table 6) have some of the most negative ε_{Nd} compositions.

Origin of Jericho diamond- and zircon-bearing eclogites

There is much debate regarding the origin of kimberlite-borne eclogites. The three main hypotheses include: (1) mantle cumulates (e.g. Smyth *et al.*, 1989, and references therein); (2) relicts of primary terrestrial differentiation soon after accretion (e.g. McCulloch, 1989); (3) relicts of subducted oceanic crust (e.g. Helmstaedt & Doig, 1975).

The Jericho diamond-bearing eclogites have a massive texture with remarkably uniform high-MgO garnet and clinopyroxene compositions (Table 2). There is a close match with the garnet and clinopyroxene compositions reported for other high-MgO eclogites, especially those recovered from the Koidu kimberlite, Sierra Leone (Hills & Haggerty, 1989). Based on mineral chemistry and oxygen isotope data, the Koidu high-MgO eclogites were interpreted to have a cumulate origin; from trace element modeling these eclogites were subdivided into low-pressure (<1 GPa) and high-pressure (2–3 GPa) suites (Barth *et al.*, 2002). The high-pressure suite was interpreted to have originated as garnet–clinopyroxene cumulates, whereas the low-pressure suite was considered to have originated as plagioclase–pyroxene–olivine cumulates (olivine gabbros and troctolites) in the basal section of subducted oceanic crust. Although it is not possible at this point to quantify paleopressures for the Jericho diamond-bearing eclogites, their origin either as ultramafic mantle cumulates or as metamorphosed olivine gabbros is possible. An ultramafic mantle cumulate origin is in agreement with the conclusion of Cookenboo *et al.* (1998*a*) that the consistent high-MgO composition and narrow range of equilibration temperatures of 1010 ± 20°C for the Jericho diamond-bearing

eclogites probably reflect derivation from a thin mantle layer of remelted peridotite at considerable depth (>180 km).

The reconstructed whole-rock compositions for Jericho zircon-bearing eclogites MX8 and MX10 reflect the unusually high FeO content of the garnet and the higher than normal Na_2O and Al_2O_3 contents of the clinopyroxene, indicating that their protoliths were probably derived from basalts with high FeO, Na_2O, and Al_2O_3 contents. The high-Na_2O and high-Al_2O_3 reconstructed bulk-rock compositions, slightly positive Eu anomaly, and occurrence of high-Al_2O_3 rutile all point to the presence of significant plagioclase in the original protolith. In addition to plagioclase, the protolith mineralogy probably consisted of clinopyroxene and ilmenite, hinting at a high-Al basalt or anorthositic gabbro parent (Emslie, 1978). The +0·7 ε_{Nd} bulk-rock composition obtained for MX1 is considered a minimum estimate and points to a protolith with a depleted mantle signature. Kopylova *et al.* (2001) identified some massive bimineralic eclogites at Jericho with flat REE profiles (∼10× chondrite) that they interpreted as fragments of N-type MORB; this provides further evidence for a depleted mantle signature preserved in some Jericho eclogites. The Jericho zircon-bearing eclogites are compositionally most akin to a suite of lawsonite-bearing eclogites from ultramafic diatremes in the Four Corners region, USA (Helmstaedt & Doig, 1975; Helmstaedt & Schulze, 1989). These distinctly Group C eclogites are compositionally similar to Franciscan eclogites on the Earth's surface and therefore probably have an origin linked to subducted oceanic lithosphere.

The U–Pb zircon dates obtained for all xenoliths in this study indicate Paleoproterozoic minimum dates for the formation of eclogite; based on the least disturbed dataset from xenolith JDLGS021-MX10 (Fig. 9c) eclogite metamorphism probably occurred a short time prior to 1785 Ma. If so, these unique eclogite xenoliths could represent pieces of subducted oceanic crust that date from the time of building the 1·88–1·84 Ga Great Bear magmatic arc (Hildebrand *et al.*, 1987). Models for the tectonic evolution of the Wopmay Orogen located on the west side of the Slave craton propose that arc magmatism is linked to east-dipping subduction of oceanic crust that ultimately culminated in the collision of the Hottah Terrane and the Slave craton (Hildebrand *et al.*, 1987).

Further support for the existence of preserved remnants of this subducted oceanic crust was revealed from detailed seismic reflection surveys along part of the SNORCLE line between Fort Simpson and Yellowknife (Cook *et al.*, 1999). This survey revealed some very pronounced east-dipping reflectors that extend from the base of the crust to about 100 km depth beneath the Great Bear magmatic arc that were interpreted to represent a subduction surface related to arc development. Another prominent reflector (M2) was identified ∼70–80 km beneath the western Slave craton (Cook *et al.*, 1999). Although this mantle reflector is nearly horizontal, it was interpreted to represent a mantle fault or a flat subduction zone with little associated arc volcanism (Cook *et al.*, 1999). Another possibility is that the M2 mantle reflector could represent the development of mafic or ultramafic sills. The projection of this mantle reflector north of the seismic line would place it directly below the Jericho region, and the depth of the reflector coincides well with estimates for depth of derivation for some Jericho eclogites (Kopylova *et al.*, 1998*b*). However, estimated depths for derivation for the majority of Jericho eclogites, including those studied here, are somewhat deeper at 150–180 km (Kopylova *et al.*, 2001). Teleseismic P-wave imaging beneath the Slave craton (Bostock, 1997) indicates three high-velocity zones at ∼75, 135 and 195 km depth, which have been interpreted to reflect a structural origin involving subduction of oceanic crust. The 195 km high-velocity zone identified by Bostock (1997) corresponds closely to the estimated depth of derivation for the zircon- and diamond-bearing eclogites examined in this study.

Paleoproterozoic mafic magmatism that is of similar age to the zircon upper intercept dates includes the 1706–1714 Ma Bonnet Plume River syenite to diorite dykes and stocks that intrude the Wernecke Supergroup in the Wernecke Mountains, Yukon (Thorkelson *et al.*, 2001); however, these exposed intrusions are quite distant from the Jericho area (∼600 km NW). If the M2 reflector corresponds to a major mafic or ultramafic sill complex then it is most probably related to the 1·27 Ga Mackenzie Igneous Event, as the Jericho kimberlites are relatively close to the focal region of this magmatism (LeCheminant & Heaman, 1989). If this is the correct interpretation of the M2 reflector, then this is not the source of the Jericho eclogites, as they have much older protolith ages. Considering the mineral chemistry, the age of eclogite metamorphism and the presence of a major mantle reflector beneath the Jericho region, we surmise that the majority of Jericho zircon-bearing eclogites are fragments of Paleoproterozoic subducted oceanic crust with an alkali basalt or anorthositic gabbro composition, whereas the diamond-bearing eclogites represent cumulates from deep mantle mafic or ultramafic sills.

CONCLUSIONS

The Jericho kimberlite JD-1 contains a large proportion of mantle xenoliths, including abundant eclogite, and represents a valuable source of information on the nature of the Slave craton lithospheric mantle. The emplacement ages for Jericho kimberlites JD-1 and JD-3 was

determined by four radiometric techniques: (1) Rb–Sr phlogopite megacrysts (173·3 ± 1·3 Ma); (2) U–Pb perovskite (176·6 ± 3·2 Ma); (3) U–Pb eclogite rutile/garnet (172·8 ± 3·2 Ma); (4) U–Pb zircon lower intercept projection (178 ± 5 Ma). All four techniques yield ages within analytical uncertainty. The preferred emplacement age for both JD1 and JD3 is 173·3 ± 1·3 Ma, the Rb–Sr phlogopite megacryst age.

A unique suite of zircon-bearing eclogites from Jericho display an extreme enrichment in HFSE that requires a complex origin, involving metamorphism and at least two stages of metasomatism. These eclogites record 950–1020°C equilibration temperatures, similar to Jericho diamond-bearing eclogites (990–1030°C), indicating derivation from similar paleodepths of ~150–180 km. Reconstructed protolith compositions indicate a range of basaltic precursors (SiO_2 varies between 40·3 and 46·8 wt %) that are characterized by their high contents of FeO (14·6–20·1 wt %), Na_2O (2·32–4·54 wt %) and Al_2O_3 (16·3–18·8 wt %). Additional support for a high-Al_2O_3 protolith is provided by the slight positive Eu anomalies (plagioclase accumulation) and the relatively high-Al_2O_3 composition of the eclogite rutile. The least modified Nd isotope composition (ε_{Nd} of +0·7) is interpreted as a minimum estimate for the protolith and indicates derivation from a depleted mantle source.

In addition to some interaction with kimberlite magma causing perturbations in major element whole-rock compositions (e.g. extreme MgO enrichment) and pervasive serpentinization of clinopyroxene, the Jericho eclogites experienced multiple episodes of metasomatism. The consistency of the model Nd ages between 1·0 and 1·3 Ga indicates that a major episode of LREE enrichment occurred at this time and is probably linked to carbonatite-type metasomatism, possibly accompanying major Proterozoic magmatism, such as the 1·27 Ga Mackenzie Igneous Event. A much older metasomatic event is responsible for the extreme HFSE enrichment and is associated with growth of zircon and rutile. One possible vestige of this event is the preservation of an armalcolite inclusion in rutile. The oldest U–Pb zircon upper intercept age of 1786 Ma is interpreted as a minimum age for zircon growth and eclogite metamorphism.

We envisage a multi-stage evolution for the generation of these unusual zircon-bearing eclogite xenoliths prior to final entrainment in the 173 Ma Jericho kimberlite: (1) emplacement of >1·79 Ga basaltic material in the Slave subcontinental mantle at depths of ~150–180 km as pieces of frozen Paleoproterozoic oceanic crust related to east-dipping subduction beneath the Slave Craton; (2) Paleoproterozoic HFSE enrichment (Type 1 metasomatism) and the growth of zircon and niobian rutile during eclogite metamorphism; (3) Mesoproterozoic invasion of carbonatite-like fluids or magmas (Type 2 metasomatism) and growth of apatite, ± carbonate, ± phlogopite and other alteration minerals in the period 1·0–1·3 Ga; (4) final interaction with the host Jericho kimberlite.

REFERENCES

Aulbach, S., Griffin, W. L., Pearson, N. J., O'Reilly, S. Y., Kivi, K. & Doyle, B. J. (2003). Origins of eclogites beneath the central Slave Craton. *Extended Abstracts, 8th International Kimberlite Conference, Victoria, B.C.*, 5 pp.

Barth, M. G., Rudnick, R. L., Horn, I., McDonough, W. F., Spicuzza, M. J., Valley, J. W. & Haggerty, S. E. (2001). Geochemistry of xenolithic eclogites from West Africa, Part I: A link between low MgO eclogites and Archean crust formation. *Geochimica et Cosmochimica Acta* **65**, 1499–1527.

Barth, M. G., Rudnick, R. L., Horn, I., McDonough, W. F., Spicuzza, M. J., Valley, J. W. & Haggerty, S. E. (2002). Geochemistry of xenolithic eclogites from West Africa, Part 2: Origins of the high MgO eclogites. *Geochimica et Cosmochimica Acta* **66**, 4325–4346.

Beard, B. L., Fraracci, K. N., Taylor, L. A., Snyder, G. A., Clayton, R. A., Mayeda, T. K. & Sobolev, N. V. (1996). Petrography and geochemistry of eclogites from the Mir kimberlite, Yakutia, Russia. *Contributions to Mineralogy and Petrology* **125**, 293–310.

Black, L. P., Kinny, P. D. & Sheraton, J. W. (1991). The difficulties of dating mafic dykes: an Antarctic example. *Contributions to Mineralogy and Petrology* **109**, 183–194.

Bossart, P. J., Meier, M., Oberli, F. & Steiger, R. H. (1986). Morphology versus U–Pb systematics in zircon: a high-resolution isotopic study of zircon population from a Variscan dike in Central Alps. *Earth and Planetary Science Letters* **78**, 339–354.

Bostock, M. G. (1997). Anisotropic upper-mantle stratigraphy and architecture of the Slave craton. *Nature* **390**, 392–395.

Brown, R. W., Allsopp, H. L., Bristow, J. W. & Smith, C. B. (1989). Improved precision of Rb–Sr dating of kimberlitic micas: an assessment of a leaching technique. *Chemical Geology* **79**, 125–136.

Cameron, A. E., Smith, D. E. & Walker, R. L. (1969). Mass spectrometry of nanogram size samples of lead. *Analytical Chemistry* **41**, 525–526.

Carswell, D. A., Dawson, J. B. & Gibb, F. G. F. (1981). Equilibrium conditions of upper-mantle eclogites: implications for kyanite-bearing and diamondiferous varieties. *Mineralogical Magazine* **44**, 79–89.

Cavell, P. A. & Baadsgaard, H. (1986). Geochronology of the Big Spruce Lake alkaline intrusion. *Canadian Journal of Earth Sciences* **23**, 1–10.

Chen, Y. D., O'Reilly, S. Y., Kinny, P. D. & Griffin, W. L. (1994). Dating lower crust and upper mantle events: an ion microprobe study of xenoliths from kimberlitic pipes, South Australia. *Lithos* **32**, 77–94.

Cherniak, D. J. (2000). Pb diffusion in rutile. *Contributions to Mineralogy and Petrology* **139**, 198–207.

Cherniak, D. J. & Watson, E. B. (2001). Pb diffusion in zircon. *Chemical Geology* **172**, 5–24.

Coleman, R. G., Lee, D. E., Beatty, L. B. & Brannock, W. W. (1965). Eclogites and eclogites: their differences and similarities. *Geological Society of America Bulletin* **76**, 483–508.

Cook, F. A., van der Velden, A. J. & Hall, K. W. (1999). Frozen subduction in Canada's Northwest Territories: Lithoprobe deep lithospheric reflection profiling of the western Canadian Shield. *Tectonics* **18**, 1–24.

Cookenboo, H. O. (1998a). The Jericho and JD-3 kimberlite pipes in the central Slave craton, Northern Canada. *Pathways '98 Extended Abstract, Vancouver, B.C.*, pp. 157–158.

Cookenboo, H. O. (1998b). Emplacement history of the Jericho kimberlite pipe, northern Canada. *Extended Abstracts, 7th International Kimberlite Conference, Cape Town*, pp. 161–163.

Cookenboo, H. O., Kopylova, M. G. & Daoud, D. K. (1998a). A chemically and texturally distinct layer of diamondiferous eclogite beneath the central Slave craton, Northern Canada. *Extended Abstracts, 7th International Kimberlite Conference, Cape Town*, pp. 164–166.

Cookenboo, H. O., Orchard, M. J. & Daoud, D. K. (1998b). Remnants of Paleozoic cover on the Archean Canadian Shield: limestone xenoliths from kimberlite in the central Slave Craton. *Geology* **26**, 391–394.

Coughlan, R. A. N. (1990). Studies in diffusional transport: grain boundary transport of oxygen in feldspars, strontium and the REEs in garnet, and thermal histories of granitic intrusions in south–central Maine using oxygen isotopes. Ph.D. thesis, Brown University, Providence, RI.

Creaser, R. A., Heaman, L. M. & Erdmer, P. (1997). Timing of high-pressure metamorphism in the Yukon–Tanana terrane, Canadian Cordillera: constraints from U–Pb zircon dating of eclogite from the Teslin Tectonic Zone. *Canadian Journal of Earth Sciences* **34**, 709–715.

Creaser, R. A., Grutter, H., Carlson, J. & Crawford, B. (2004). Macrocrystal phlogopite Rb–Sr dates for the Ekati property kimberlites, Slave Province, Canada: evidence for multiple intrusive episodes in the Paleocene and Eocene. *Lithos* **76**, 399–414.

Dalton, J. & Blundy, J. (2000). Carbonatites from recycled eclogites. *Abstract Volume, Goldschmidt 2000 Conference, Oxford, UK*, p. 330.

Davis, W. J. (1997). U–Pb zircon and rutile ages from granulite xenoliths in the Slave province: evidence for mafic magmatism in the lower crust coincident with Proterozoic dike swarms. *Geology* **25**, 343–346.

Dawson, J. B. & Smith, J. V. (1977). The MARID (mica–amphibole–rutile–ilmenite–diopside) suite of xenoliths in kimberlite. *Geochimica et Cosmochimica Acta* **41**, 309–323.

Dowall, D. P., Pearson, D. G., Nowell, G. M., Kjarsgaard, B. A., Armstrong, J. & Horstwood, M. S. A. (2003). Comparative

geochemistry of kimberlites from the Lac de Gras field, NWT—an integrated isotopic and elemental study. *Extended Abstracts, 8th International Kimberlite Conference, Victoria, B.C.*, 5 pp.

Ellis, D. J. & Green, D. H. (1979). An experimental study of the effect of Ca upon garnet–clinopyroxene Fe–Mg exchange equilibria. *Contributions to Mineralogy and Petrology* **71**, 13–33.

Emslie, R. F. (1978). Elsonian magmatism in Labrador: age, characteristics and tectonic setting. *Canadian Journal of Earth Sciences* **15**, 438–453.

Erlank, A. J., Waters, F. G., Hawkesworth, C. J., Haggerty, S. E., Allsopp, H. L., Rickard, R. S. & Menzies, M. A. (1987). Evidence for mantle metasomatism in peridotite nodules from the Kimberley pipes, South Africa. In: Menzies, M. A. & Hawkesworth, C. J. (eds) *Mantle Metasomatism*. New York: Academic Press, pp. 221–311.

Fung, A. T. (1998). Petrochemistry of upper mantle eclogites from the Grizzly, Leslie, Pigeon and Sable kimberlites in the Slave Province, Canada. *Extended Abstracts, 7th International Kimberlite Conference, Cape Town*, pp. 230–232.

Green, D. H. (1966). The origin of the 'eclogites' from Salt Lake Crater, Hawaii. *Earth and Planetary Science Letters* **1**, 414–420.

Haggerty, S. E. (1983). The mineral chemistry of new titanates from the Jagersfontein kimberlite, South Africa: implications for metasomatism in the upper mantle. *Geochimica et Cosmochimica Acta* **47**, 1833–1854.

Haggerty, S. (1992). Oxide mineralogy of the upper mantle. In: Donald H. Lindsley (ed) *Oxide Minerals: Petrologic and Magnetic Significance. Mineralogical Society of America, Reviews of Mineralogy* **25**, 355–416.

Haggerty, S. (1994). Superkimberlites: a geodynamic window to the Earth's core. *Earth and Planetary Science Letters* **122**, 57–69.

Hamilton, M. A., Pearson, D. G., Stern, R. A. & Boyd, F. R. (1998). Constraints on MARID petrogenesis: SHRIMP II U–Pb zircon evidence for pre-eruption metasomatism at Kampfersdam. *Extended Abstracts, 7th International Kimberlite Conference, Cape Town*, pp. 296–298.

Harlan, S. S., Heaman, L. M., LeCheminant, A. N. & Premo, W. R. (2003). Gunbarrel mafic magmatic event: a key 780 Ma time marker for Rodinia plate reconstructions. *Geology* **31**, 1053–1056.

Harrison, W. J. & Wood, B. J. (1980). An experimental investigation of the partitioning of REE between garnet and liquid with reference to the role of defect equilibria. *Contributions to Mineralogy and Petrology* **72**, 145–155.

Hart, S. R. (1964). The petrology and isotopic–mineral age relations of a contact zone in the Front Range, Colorado. *Journal of Geology* **72**, 493–525.

Heaman, L. M. & Kjarsgaard, B. (2000). Timing of eastern North American kimberlite magmatism: continental extension of the Great Meteor hotspot track? *Earth and Planetary Science Letters* **178**, 253–268.

Heaman, L. M. & LeCheminant, A. N. (1993). Paragenesis and U–Pb systematics of baddeleyite (ZrO$_2$). *Chemical Geology* **110**, 95–126.

Heaman, L. M. & Machado, N. (1992). Timing and origin of mid-continent rift alkaline magmatism, North America: evidence from the Coldwell Complex. *Contributions to Mineralogy and Petrology* **110**, 289–303.

Heaman, L. M. & Parrish, R. R. (1991). U–Pb geochronology of accessory minerals. In: Heaman, L. M. & Ludden, J. N. (eds) *Applications of Radiogenic Isotope Systems to Problems in Geology. Mineralogical Association of Canada, Short Course Handbook* **19**, 59–102.

Heaman, L. M., LeCheminant, A. N. & Rainbird, R. H. (1992). Nature and timing of Franklin Igneous Events, Canada: implications for a Late Proterozoic mantle plume and the break-up of Laurentia. *Earth and Planetary Science Letters* **109**, 117–131.

Heaman, L. M., Kjarsgaard, B. A., Creaser, R. A., Cookenboo, H. O. & Kretschmar, U. (1997). Multiple episodes of kimberlite

magmatism in the Slave Province, North America. *Lithoprobe Workshop Report* **56**, 14–17.

Heaman, L. M., Creaser, R. A. & Cookenboo, H. O. (2002). Extreme enrichment of high field strength elements in Jericho eclogite xenoliths: a cryptic record of Paleoproterozoic subduction, partial melting, and metasomatism beneath the Slave craton, Canada. *Geology* **30**, 507–510.

Heaman, L. M., Kjarsgaard, B. A. & Creaser, R. A. (2003). The timing of kimberlite magmatism in North America: implications for global kimberlite genesis and diamond exploration. *Lithos* **71**, 153–184.

Heaman, L. M., Kjarsgaard, B. A. & Creaser, R. A. (2004). The temporal evolution of North American kimberlites. *Lithos* **76**, 377–397.

Helmstaedt, H. & Doig, R. (1975). Eclogite nodules from kimberlite pipes in the Colorado plateau—samples of subducted Franciscan type oceanic lithosphere. *Physics and Chemistry of the Earth* **9**, 95–111.

Helmstaedt, H. & Schulze, D. J. (1989). Eclogite-facies ultramafic xenoliths from Colorado Plateau diatreme breccias: comparison with eclogites in crustal environments, evaluation of the subduction hypothesis, and implications for eclogite xenoliths from diamondiferous kimberlites. In: Smith, D. (ed.) *Eclogite-Facies Rocks.* Amsterdam: Elsevier, pp. 358–368.

Hetman, C., Scott-Smith, B., Webb, K. & Kirkley, M. (2003). De Beers Canada Large Core Exhibit Report. *8th International Kimberlite Conference, Victoria, B.C., Canada.*

Hildebrand, R. S., Hoffman, P. F. & Bowring, S. (1987). Tectono-magmatic evolution of the 1·9 Ga Great Bear magmatic zone, Wopmay orogen, northwestern Canada. *Journal of Volcanology and Geothermal Research* **32**, 99–118.

Hills, D. V. & Haggerty, S. E. (1989). Petrochemistry of eclogites from the Koidu kimberlite complex, Sierra Leone. *Contributions to Mineralogy and Petrology* **103**, 397–422.

Hogarth, D. D. (1989). Pyrochlore, apatite and amphibole: distinctive minerals in carbonatite. In: Bell, K. (ed.) *Carbonatites: Genesis and Evolution.* London: Unwin Hyman, pp. 105–148.

Ionov, D. A., Dupuy, C., O'Reilly, S. Y., Kopylova, M. G. & Genshaft, Y. S. (1993). Carbonated peridotite xenoliths from Spitsbergen: implications for trace element signature of mantle carbonate metasomatism. *Earth and Planetary Science Letters* **119**, 283–297.

Irvine, G. J., Pearson, D. G. & Carlson, R. W. (1999). Age of lithospheric mantle beneath and around the Slave craton: a rhenium–osmium isotopic study of peridotite xenoliths from the Jericho and Somerset Island kimberlites. *Program with Abstracts, 9th Annual V. M. Goldschmidt Conference* **971**, 134–145.

Irvine, G. J., Pearson, D. G. & Carlson, R. W. (2001). The age of two cratons: a PGE and Os-isotopic study of peridotite xenoliths from the Jericho kimberlite (Slave Craton) and the Somerset Island kimberlite field (Churchill Province). *The Slave–Kaapvaal Workshop, Merrickville, Ont., Canada.*

Jacob, D. E. (2004). Nature and origin of eclogite xenoliths from kimberlites. *Lithos* **77**, 295–316.

Jacob, D. E., Fung, A., Jagoutz, E. & Pearson, D. G. (2003). Petrology and geochemistry of eclogite xenoliths from the Ekati kimberlites area. *Extended Abstracts, 8th International Kimberlite Conference, Victoria, B.C.,* 1 p.

Jacob, D. E., Bizimis, M. & Salters, V. J. M. (2005). Lu–Hf and geochemical systematics of recycled ancient oceanic crust: evidence from Roberts Victor eclogites. *Contributions to Mineralogy and Petrology* **148**, 707–720.

Jagoutz, E. (1988). Nd and Sr systematics in an eclogite xenolith from Tanzania: evidence for frozen mineral equilibria in the continental lithosphere. *Geochimica et Cosmochimica Acta* **52**, 1285–1293.

Jaques, A. L., Haggerty, S. E., Lucas, J. & Boxer, G. L. (1989). Mineralogy and petrology of the Argyle (AK-1) lampröites pipe, Western Australia. In: Ross, J. (ed.) *Proceedings of the Fourth International Kimberlite Conference 1. Geological Society of Australia Special Publication* **14**, 153–170.

Jarosewich, E. (2002). *Journal of Research of the National Institute of Standards and Technology* **107**, 681–885.

Jerde, E. A., Taylor, L. A., Crozaz, G., Sobolev, N. V. & Sobolev, V. N. (1993). Diamondiferous eclogites from Yakutia, Siberia: evidence for a diversity of protoliths. *Contributions to Mineralogy and Petrology* **114**, 189–202.

Jordan, T. H. (1988). Structure and formation of the continental tectosphere. *Journal of Petrology, Special Volume*, 11–37.

Kinny, P. D. & Dawson, J. B. (1992). A mantle metasomatic injection event linked to late Cretaceous kimberlite magmatism. *Nature* **360**, 726–728.

Kinny, P. D., Compston, W., Bristow, J. W. & Williams, I. S. (1989). Archean mantle xenocrysts in a Permian kimberlite: two generations of kimerlitic zircon in Jwaneng DK2, southern Botswana. In: Ross, J. (ed.) *Proceedings of the Fourth International Kimberlite Conference 2, Kimberlites and Related Rocks: their Mantle/Crustal Setting, Diamonds and Diamond Exploration. Geological Society of Australia Special Publication* **14**, 833–842.

Kopylova, M. G. & Caro, G. (2004). Mantle xenoliths from the southeastern Slave Craton: evidence for chemical zonation in a thick, cold lithosphere. *Journal of Petrology* **45**, 1045–1067.

Kopylova, M. G. & Russell, J. K. (2000). Chemical stratification of cratonic lithosphere: constraints from the Northern Slave craton, Canada. *Earth and Planetary Science Letters* **181**, 71–87.

Kopylova, M. G., Russell, J. K. & Cookenboo, H. (1998a). Petrography and chemistry of the Jericho kimberlite (Slave Craton, Northern Canada). *Extended Abstracts, 7th International Kimberlite Conference, Cape Town*, pp. 449–451.

Kopylova, M. G., Russell, J. K. & Cookenboo, H. (1998b). Upper-mantle stratigraphy of the Slave craton, Canada: insights into a new kimberlite province. *Geology* **26**, 315–318.

Kopylova, M. G., Russellxs, J. K. & Cookenboo, H. (1999a). Mapping the lithosphere beneath the North Central Slave Craton. *Proceedings of the 7th International Kimberlite Conference, Cape Town, Volume 1: The J. B. Dawson Volume*, pp. 468–479.

Kopylova, M. G., Russell, J. K. & Cookenboo, H. (1999b). Petrology of peridotite and pyroxenite xenoliths from the Jericho kimberlite: implications for the thermal state of the mantle beneath the Slave craton, northern Canada. *Journal of Petrology* **40**, 79–104.

Kopylova, M. G., Russell, J. K. & Christensen, N. I. (2001). Composition and fabric of the Northern Slave eclogite as evidence for mantle metasomatism. *Lithoprobe Report 81, Proceedings from Pan-Lithoprobe Workshop III: Mantle Lithosphere and Lithoprobe: Views of Continental Evolution from the Bottom Up*, pp. 61–70.

Kopylova, M. G., Lo, J. & Christensen, N. I. (2004). Petrological constraints on seismic properties of the Slave upper mantle (Northern Canada). *Lithos* **77**, 493–510.

Kresten, P., Fels, P. & Berggren, G. (1975). Kimberlitic zircons—a possible aid in prospecting for kimberlites. *Mineralium Deposita* **10**, 47–56.

Krogh, T. E. (1973). A low-contamination method for hydrothermal decomposition of zircon and extraction of U and Pb for isotopic age determinations. *Geochimica et Cosmochimica Acta* **37**, 485–494.

Krogh-Ravna, E. (2000). The garnet–clinopyroxene Fe^{+2}:Mg geothermometer: an updated calibration. *Journal of Metamorphic Geology* **18**, 211–219.

Kushiro, I. & Aoki, K.-I. (1968). Origin of some eclogite inclusions in kimberlite. *American Mineralogist* **53**, 1347–1367.

LeCheminant, A. N. & Heaman, L. M. (1989). Mackenzie Igneous Events, Canada: Middle Proterozoic hotspot magmatism associated with ocean opening. *Earth and Planetary Science Letters* **96**, 38–48.

LeCheminant, A. N. & Heaman, L. M. (1994). 779 Ma mafic magmatism in the northwestern Canadian Shield and northern Cordillera: a new regional time-marker. *Program with Abstracts, 8th International Conference on Geochronology and Isotope Geology, Berkeley, California. US Geological Survey Circular* **1107**, 187.

Lee, J. K. W., Williams, I. S. & Ellis, D. J. (1997). Pb, U and Th diffusion in natural zircon. *Nature* **390**, 159–162.

Ludwig, K. R. (1992). ISOPLOT—a plotting and regression program for radiogenic isotope data, version 2.57. *US Geological Survey Open-File Report* **91**, 445.

Macdonald, G. A. & Katsura, T. (1964). Chemical composition of Hawaiian lavas. *Journal of Petrology* **5**, 82–133.

MacGregor, I. D. & Carter, J. L. (1970). The chemistry of clinopyroxenes and garnets from the Roberts Victor mine, South Africa. *Physics of the Earth and Planetary Interiors* **3**, 391–397.

MacGregor, I. D. & Manton, W. I. (1986). Roberts Victor eclogites: ancient oceanic crust. *Journal of Geophysical Research* **91**, 14063–14079.

McCandless, T. E. & Gurney, J. J. (1989). Sodium in garnet and potassium in clinopyroxene: criteria for classifying mantle eclogites. In: Ross, J. (ed.) *Kimberlites and Related Rocks, Volume 2. Their Mantle/Crust Setting, Diamonds and Diamond Exploration. Geological Society of Australia Special Publication* **14**, 827–832.

McCulloch, M. T. (1989). Sm–Nd systematics in eclogite and garnet peridotite nodules from kimberlites: implications for the early differentiation of the earth. In: Ross, J. (ed.) *Kimberlites and Related Rocks, Volume 2. Their Mantle/Crust Setting, Diamonds and Diamond Exploration. Geological Society of Australia Special Publication* **14**, 864–876.

McGetchin, T. R. & Silver, L. T. (1972). A crustal-upper mantle model for the Colorado plateau based on observations of crystalline rock fragments in the Moses Rock dike. *J. Geophys. Res.* **77**, 7022–7037.

Meyer, H. O. A. & Boctor, N. Z. (1975). Sulfide–oxide minerals in eclogite from Stockdale kimberlite, Kansas. *Contributions to Mineralogy and Petrology* **52**, 57–68.

Mezger, K., Hanson, G. N. & Bohlen, S. R. (1989). High-precision U–Pb ages of metamorphic rutile: application to the cooling history of high-grade terranes. *Earth and Planetary Science Letters* **96**, 106–118.

Mitchell, R. H. (1986). *Kimberlites: Mineralogy, Geochemistry and Petrology.* New York: Plenum, 442 pp.

Nassichuk, W. W. & McIntyre, D. J. (1995). Cretaceous and Tertiary fossils discovered in kimberlites at Lac de Gras in the Slave province, Northwest Territories. *Geological Survey of Canada Current Research* **1995-B**, 109–114.

Neal, C. R., Taylor, L. A., Davidson, J. P., Holden, P., Halliday, A. N., Nixon, P. H., Paces, J. B., Clayton, R. N. & Mayeda, T. K. (1990). Eclogites with oceanic crustal and mantle signatures from the Bellsbank kimberlite, South Africa, Part 2: Sr, Nd, and O isotope geochemistry. *Earth and Planetary Science Letters* **99**, 362–379.

Nicolaysen, L. O. (1957). Solid diffusion in radioactive minerals and the measurement of absolute time. *Geochimica et Cosmochimica Acta* **11**, 41–59.

O'Reilly, S. Y. & Griffin, W. L. (2000). Apatite in the mantle: implications for metasomatic processes and high heat production in Phanerozoic mantle. *Lithos* **53**, 217–232.

Paquette, J. L., Peucat, J. J., Bernard-Griffiths, J. & Marchand, J. (1985). Evidence for old Precambrian relics shown by U–Pb zircon dating of eclogites and associated rocks in the Hercynian belt of South Brittany, France. *Chemical Geology* **52**, 203–216.

Paquette, J. L., Monchoux, P. & Couturier, M. (1995). Geochemical and isotopic study of a norite–eclogite transition in the European Variscan belt: implications for U–Pb zircon systematics in metabasic rocks. *Geochimica et Cosmochimica Acta* **59**, 1611–1622.

Pearce, J. A., Baker, P. E., Harvey, P. K. & Luff, I. W. (1995). Geochemical evidence for subduction fluxes, mantle melting and fractional crystallization beneath the South Sandwich Island Arc. *Journal of Petrology* **36**, 1073–1109.

Pearson, D. G. (1999). The age of continental roots. *Lithos* **48**, 171–194.

Pearson, N. J., Griffin, W. L., Doyle, B. J., O'Reilly, S. Y., van Achterbergh, E. & Kivi, K. (1999). Xenoliths from kimberlite pipes of the Lac de Gras area, Slave Craton, Canada. In: Gurney, J. J., Gurney, J. L., Pascoe, M., Richardson, S. H. (eds) *Proceedings of the 7th International Kimberlite Conference, Cape Town.* Cape Town: Red Roof Design, pp. 644–658.

Peucat, J. J., Vidal, Ph., Godard, G. & Postaire, B. (1982). Precambrian U–Pb zircon ages in eclogites and garnet pyroxenites from South Brittany (France): an old oceanic crust in the West European Hercynian belt? *Earth and Planetary Science Letters* **60**, 70–78.

Price, S. E., Russell, J. K. & Kopylova, M. G. (2000). Primitive magma from the Jericho pipe, N. W. T., Canada: constraints on primary kimberlite melt chemistry. *Journal of Petrology* **41**, 789–808.

Rudnick, R. L., McDonough, W. F. & Chappell, B. W. (1993). Carbonatite metasomatism in the northern Tanzanian mantle: petrographic and geochemical characteristics. *Earth and Planetary Science Letters* **114**, 463–475.

Rudnick, R. L., Ireland, T. R., Gehrels, G., Irving, A. J., Chesley, J. T. & Hanchar, J. M. (1998). Dating mantle metasomatism: U–Pb geochronology of zircons in cratonic mantle xenoliths from Montana and Tanzania. *Extended Abstracts, 7th International Kimberlite Conference, Cape Town*, pp. 754–756.

Rudnick, R. L., Ireland, T. R., Gehrels, G., Irving, A. J., Chesley, J. T. & Hanchar, J. M. (1999). Dating mantle metasomatism: U–Pb geochronology of zircons in cratonic mantle xenoliths from Montana and Tanzania. In: Gurney, J. J., Gurney, J. L., Pascoe, M. D. & Richardson, S. H. (eds) *Proceedings of the 7th International Kimberlite Conference 2, Cape Town.* Cape Town: Red Roof Design, pp. 728–735.

Rudnick, R. L., Barth, M., Horn, I. & McDonough, W. F. (2000). Rutile-bearing refractory eclogites: missing link between continents and depleted mantle. *Science* **287**, 278–281.

Schmidberger, S. S., Heaman, L. M., Simonetti, A. & Creaser, R. A. (2004). Lu–Hf systematics of kimberlite-hosted eclogite xenoliths from South Africa and Canada. *Abstracts, 13th Annual V. M. Goldschmidt Conference, Copenhagen. Geochimica et Cosmochimica Acta, Supplement*, A610.

Schmitz, M., Shirey, S., & Carlson, R. (2003). High-precision U-Pb geochronology and Lu-Hf isotopic systematics of zircons in southern African cratonic mantle eclogites and implications for subcontinental lithospheric mantle evolution and metasomatism. *Extended Abstracts, 8th International Kimberlite Conference, Victoria, B. C.*, 1p.

Shervais, J. W., Taylor, L. A., Lugmair, G. W., Clayton, R. N., Mayeda, T. K. & Korotev, R. L. (1988). Early Proterozoic oceanic crust and the evolution of the subcontinental mantle: eclogites and related rocks from southern Africa. *Geological Society of America Bulletin* **100**, 411–423.

Smith, C. B. (1983). Pb, Sr and Nd isotopic evidence for sources of southern African Cretaceous kimberlites. *Nature* **304**, 51–54.

Smith, J. V. & Dawson, J. B. (1975). Chemistry of Ti-poor spinels, ilmenites and rutiles from peridotite and eclogite xenoliths. *Physics and Chemistry of the Earth* **9**, 309–322.

Smyth, J. R., Caporuscio, F. A. & McCormick, T. (1989). Mantle eclogites: evidence of igneous fractionation in the mantle. *Earth and Planetary Science Letters* **93**, 133–141.

Snyder, G. A., Taylor, L. A., Crozaz, G., Halliday, A. N., Beard, B. L., Sobolev, V. N. & Sobolev, N. V. (1997). The origins of Yakutian eclogite xenoliths. *Journal of Petrology* **38**, 85–113.

Sorensen, S. S. & Grossman, J. N. (1989). Enrichment of trace elements in garnet amphibolites from a paleo-subduction zone: Catalina Schist, southern California. *Geochimica et Cosmochimica Acta* **53**, 3155–3177.

Stacey, J. S. & Kramers, J. D. (1975). Approximation of terrestrial lead isotope evolution by a two-stage model. *Earth and Planetary Science Letters* **26**, 207–221.

Stachel, T., Brey, G. P. & Harris, J. W. (2000). Kankan diamonds (Guinea) I: From the lithosphere down to the transition zone. *Contributions to Mineralogy and Petrology* **140**, 1–15.

Sun, S.-s. & McDonough, W. F. (1989). Chemical and isotopic systematics of oceanic basalts: implications for mantle composition and processes. In: Saunders, A. D. & Norry, M. J. (eds) *Magmatism in the Ocean Basins. Geological Society, London, Special Publications* **42**, 313–345.

Taylor, L. A. & Neal, C. R. (1989). Eclogites with oceanic crustal and mantle signatures from the Bellsbank kimberlite, South Africa, Part 1: Mineralogy, petrography and whole rock chemistry. *Journal of Geology* **97**, 551–567.

Thorkelson, D. J., Mortensen, J. K., Creaser, R. A., Davidson, G. J. & Abbott, J. G. (2001). Early Proterozoic magmatism in Yukon, Canada: constraints on the evolution of northwestern Laurentia. *Canadian Journal of Earth Sciences* **38**, 1479–1494.

Tilton, G. R. (1960). Volume diffusion as a mechanism for discordant lead ages. *Journal of Geophysical Research* **65**, 2933–2945.

Tollo, R. P. & Haggerty, S. E. (1987). Nb–Cr rutile in the Orapa kimberlite, Botswana. *Canadian Mineralogist* **25**, 251–264.

Unterschutz, J. L. E., Creaser, R. A., Erdmer, P., Thompson, R. I. & Daughtry, K. L. (2002). North American margin origin of Quesnel terrane strata in the southern Canadian Cordillera: inferences from geochemical and Nd isotopic characteristics of Triassic metasedimentary rocks. *Geological Society of America Bulletin* **114**, 462–475.

Van Orman, J. A., Grove, T. L., Shimizu, N. & Layne, G. D. (2002). Rare earth element diffusion in a natural pyrope single crystal at 2·8 GPa. *Contributions to Mineralogy and Petrology* **142**, 416–424.

Villeneuve, M. E. & Relf, C. (1998). Tectonic setting of 2·6 Ga carbonatites in the Slave Province, NW Canada. *Journal of Petrology* **39**, 1975–1986.

Wasserburg, G. J. (1963). Diffusion processes in lead–uranium systems. *Journal of Geophysical Research* **68**, 4823–4846.

Watson, K. D. & Morton, D. M. (1969). Eclogite inclusions in kimberlite pipes at Garnet Ridge, northeastern Arizona. *American Mineralogist* **54**, 267–285.

Williams, A. F. (1932). *The Genesis of Diamond.* London: E. Benn.

Yaxley, G. M., Green, D. H. & Kamenetsky, V. (1998). Carbonatite metasomatism in the southeastern Australia lithosphere. *Journal of Petrology* **39**, 1917–1930.